

Moulin density controls drainage development beneath the Greenland Ice Sheet

Alison Banwell¹, Ian Hewitt², Ian Willis¹ and Neil Arnold¹

¹*Scott Polar Research Institute, University of Cambridge, Lensfield Rd, Cambridge, CB2 1ER, UK.*

²*Mathematical Institute, University of Oxford, Woodstock Rd, Oxford, OX2 6GG, UK.*

Key Points

- 1) Combining models of supra- and sub-glacial drainage is an effective way of assessing the impact of moulin density on subglacial drainage
- 2) A higher moulin density causes an earlier onset of subglacial channelization and results in a more widespread channel network across the bed
- 3) Moulin density has complex and contrasting effects on water pressure in the early and late melt season, with basal sliding implications

Abstract

Uncertainty remains about how the surface hydrology of the Greenland Ice Sheet influences its subglacial drainage system, affecting basal water pressures and ice velocities, particularly over intra- and inter-seasonal timescales. Here, we apply a high spatial (200 m) and temporal (1 h) resolution subglacial hydrological model to a marginal (extending ~25 km inland), land-terminating, ~200 km² domain in the Paakitsoq region, West Greenland. The model is based on that by Hewitt [2013], but adapted for use with both real topographic boundary conditions and calibrated modeled water inputs [Banwell *et al.* 2013]. The inputs consist of moulin hydrographs, calculated by a surface routing and lake-filling/draining model, which is forced with distributed runoff from a surface energy-balance model. Results suggest that the areal density of lake-bottom moulins, and their timing of opening during the melt season, strongly affects subglacial drainage system development. A higher moulin density causes an earlier onset of subglacial channelization (i.e. water transport through channels rather than the distributed sheet), that becomes relatively widespread across the bed, whereas a lower moulin density results in a later onset of channelization that becomes less widespread across the bed. In turn, moulin density has a strong control on spatial and temporal variations in subglacial water pressures, which will influence basal sliding rates, and thus ice motion. The density of active surface-to-bed connections should be considered alongside surface melt intensity and extent in future predictions of the ice sheet's dynamics.

Introduction

31 The Greenland Ice Sheet (GrIS), which has lost mass at an accelerating rate over the past two
32 decades, is predicted to be the largest cryospheric contributor to global sea-level rise for the rest of
33 this century [Graversen *et al.*, 2011; Hanna *et al.*, 2013]. To predict the effects of an increasingly
34 warmer climate on the GrIS, it is crucial to better understand the physical processes that govern its
35 surface and dynamic mass balance [Church *et al.*, 2013]. Seasonal acceleration and deceleration of
36 marginal areas is influenced by the dynamic response of the subglacial drainage system to spatial and
37 temporal variability in surface meltwater delivery to the bed via crevasses and moulins [Thomsen
38 and Olesen, 1989; Bartholomew *et al.*, 2012; Cowton *et al.*, 2013; Smith *et al.*, 2015], which often
39 open up as a result of surface lake drainage events [Das *et al.*, 2008; Tedesco *et al.*, 2013; Doyle *et al.*,
40 2013; Stevens *et al.*, 2015]. However, the precise manner in which surface meltwater is delivered
41 to the subglacial drainage system remains poorly understood. Similarly, there is a lack of knowledge
42 about how the subglacial drainage system responds to the spatially and temporally varying surface
43 water inputs, and how it therefore evolves to affect basal water pressure and surface ice velocity
44 [Vaughan *et al.*, 2013].

45 Numerous field- and model-based studies have been undertaken to address this lack of knowledge
46 and understanding. Field-based studies have attempted to infer the behavior of the GrIS's subglacial
47 drainage system from measurements of meteorology, borehole water-pressures, dye-tracing, and
48 surface velocity and uplift [e.g., Zwally *et al.*, 2002; Das *et al.*, 2008; Chandler *et al.*, 2013; Cowton
49 *et al.*, 2013; Doyle *et al.*, 2013; Meierbachtol *et al.*, 2013; Tedesco *et al.*, 2013; Andrews *et al.*, 2014;
50 Ryser *et al.*, 2014; Stevens *et al.*, 2015]. Several catchment-scale modeling studies have been
51 undertaken which have tended to fit into one of two approaches. The first approach has used real
52 boundary conditions and calibrated, modeled water inputs to simulate subglacial drainage for
53 specific catchments in particular years. However, a key limitation of this approach is the somewhat
54 idealized representation of the subglacial drainage system, comprising either channels only (the
55 locations of which needed to be prescribed) [e.g. Colgan *et al.*, 2011; Banwell *et al.*, 2013; Mayaud
56 *et al.*, 2014], or a weak-sediment layer/porous sheet only [e.g. Bougamont *et al.*, 2014].

57 The second modeling approach has used synthetic boundary conditions (e.g. simplified ice
58 geometry) and idealized water inputs to simulate generic conditions for typical years. This approach
59 has usually achieved a more complex representation of the subglacial drainage system, which can
60 take the form of inefficient and efficient flow in a porous sheet [e.g., de Fleurian *et al.*, 2014] or
61 inefficient flow in a sheet and efficient flow in channels [e.g. Schoof, 2010; Bartholomew *et al.*,
62 2011; Hewitt, 2013; Werder *et al.*, 2013; Hoffman and Price, 2014]. These configurations emerge
63 within the model in response to variable meltwater inputs and pressure gradients, with interaction

64 and switching between the inefficient and efficient components dependent upon water flux. To date,
65 therefore, catchment-scale hydrological models for marginal areas of the GrIS have tended to
66 sacrifice an element of reality having either: i) real topographic boundary conditions and meltwater
67 inputs but with a simplified subglacial hydrology; or ii) a more realistic representation of the
68 subglacial drainage system, but with artificial topographic boundary conditions and water inputs.

69 Here, to benefit from the advantages that both modeling approaches have offered, we develop and
70 apply a high spatial (200 m) and temporal (1 h) resolution subglacial hydrological model to a
71 drainage basin (extending ~25 km inland) within the Paakitsoq region, West Greenland. The model
72 is based on that of *Hewitt* [2013], but is adapted for use with both the real topographic boundary
73 conditions and the calibrated, modeled water inputs from *Banwell et al.* [2013] for the 2005 melt
74 season. These water inputs are in the form of moulin hydrographs, which are calculated by a surface
75 routing and lake-filling model [*Banwell et al.*, 2012b, 2013; *Arnold et al.*, 2014], combined with a
76 surface lake-drainage model [*Clason et al.*, 2012; *Banwell et al.*, 2013; *Arnold et al.*, 2014]. The
77 model is forced with distributed hourly runoff calculated by a surface mass balance (SMB) model,
78 which incorporates the surface energy-balance as well as subsurface conduction and melting and
79 refreezing in the snowpack [*Banwell et al.*, 2012a].

80 The primary aim of this study is to explore how the subglacial hydrological system of the GrIS
81 evolves in space and time in response to varying modeled moulin inputs associated with fluctuating
82 patterns of surface melt, refreezing, routing through snow and across ice, and lake drainage events. A
83 key output is the spatial and temporal variation in subglacial water pressure, which is of interest in
84 helping to explain patterns of surface velocity and uplift found in previous studies [e.g. *Das et al.*,
85 2008; *Tedesco et al.*, 2013; *Doyle et al.*, 2015]. As a secondary aim, we compare the results of the
86 current study to those from *Banwell et al.* [2013]. As the inputs and topographic boundary conditions
87 for each model are identical, any difference between the results will be due solely to the different
88 representations of the subglacial hydrology, particularly the inclusion of a distributed system in the
89 current model. Although this is the secondary aim, for continuity with the previous work, we discuss
90 this aspect first, before moving on to the more substantial primary aim of the paper.

91 **2. Study Site and Available Data**

92 The Paakitsoq region is defined as ~2,300 km² of predominantly land-terminating ice, located in
93 western Greenland, north of Jakobshavn Isbræ [*Banwell et al.*, 2013; their Figure 1). The region was
94 initially chosen by *Banwell et al.* [2012a, 2012b, 2013] and later by *Arnold et al.* [2014] and *Mayaud*
95 *et al.* [2014] due to the availability of various data sets including: (i) hourly meteorological data

measured at three GC-Net stations, JAR 1, JAR 2, and Swiss Camp [Steffen and Box, 2001]; and (ii) coastal precipitation and temperature data from the Asiaq Greenland Survey Station 437 (190 m above sea level, 4 km west of the ice margin), all of which were used to drive the SMB model [Banwell *et al.*, 2012a]; (iii) proglacial stream discharge data measured at the Asiaq station, which were used to validate the glacier hydrological model of Banwell *et al.* [2013]; and iv) a 750 m resolution bed digital elevation model (DEM) [Plummer *et al.*, 2008] for the subglacial routing model, and a 30 m resolution surface DEM taken from the Advanced Spaceborne Thermal Emission and Reflection Radiometer (ASTER) global DEM (GDEM) for the surface melt and routing models. Both DEMs were resampled to 200 m using bilinear interpolation.

The Paakitsoq region includes the areas for which the SMB model and the surface routing and lake-filling model have both been calibrated [Banwell *et al.*, 2012a; 2012b]. Additionally, the lake-drainage model has been calibrated for the entire region, through the comparison of modeled lake-volumes and drainage dates to those observed from nine Landsat 7 ETM+ satellite images [Arnold *et al.*, 2014]. In the current study, our model domain, as defined by Banwell *et al.* [2013; their Figure 1], is a $\sim 200 \text{ km}^2$ subglacial catchment within the Paakitsoq region that feeds the proglacial Asiaq gauging station (Figure 1). The proglacial discharge measured here was used by Banwell *et al.* [2013] to specifically calibrate the lake-drainage model for this 200 km^2 catchment. The domain is entirely within the ablation area of the ice sheet, extends $\sim 25 \text{ km}$ inland from the margin with a surface elevation range of $\sim 150 \text{ m}$ to $1,000 \text{ m}$, and includes ice thicknesses $< 815 \text{ m}$.

3. Methods

3.1. The Subglacial Model

The subglacial routing model is based on that developed by Hewitt [2013]. Although Hewitt's [2013] model has two distinct components, a model for subglacial water flow and a model for ice flow, we use only the subglacial water flow component in this study. This is because we lack appropriate temporally and spatially resolved data to constrain the modeled surface velocities. We focus specifically on analyzing spatial and temporal variations in subglacial water pressure in response to changing surface-derived meltwater inputs through the 2005 melt season. A brief description of the model is given below; full details are provided in Hewitt [2013; his section 2.3]. The model is almost identical to that of Werder *et al.* [2013], except for its numerical implementation.

3.1.1. Model Description

The model is implemented in a two-dimensional finite-difference framework. It is based on a continuum 'sheet', connected to discrete conduits, which are arranged along the edges and diagonals

of a rectangular mesh of nodes. For low discharge, almost all meltwater is accommodated in the distributed sheet, whereas for sufficiently high discharge, the model exhibits an instability that leads to the formation of a self-organized channel system, in which a small subset of the conduits carries most of the discharge. Water storage is accounted for in an englacial aquifer and in moulins, the latter also acting as point sources of water to the subglacial system (see section 3.2.2).

The distributed sheet is separated into a cavity sheet, with thickness $h_{cav}(x,y,t)$, and an elastic sheet, with thickness $h_{el}(x,y,t)$; both are described below. These two components are added together to obtain the overall sheet thickness $h(x,y,t) = h_{cav} + h_{el}$. This is one of two main differences to the model set-up in *Hewitt* [2013], where only one or other of these two models was used.

The cavity sheet evolves according to

$$\frac{\partial h_{cav}}{\partial t} = \frac{\rho_w}{\rho_i} m + \frac{U_b(h_r - h_{cav})}{l_r} - \frac{2A}{n^n} h_{cav} |N|^{n-1} N, \quad (1)$$

where t is time, ρ_w is water density (1000 kg m^{-3}), ρ_i is ice density (910 kg m^{-3}), h_r and l_r are bed roughness height (0.1 m) and length scales (10 m), respectively, U_b is the basal sliding speed, N is the effective pressure ($P_i - P_w$, where P_i is ice-overburden pressure and P_w is water pressure), and A and n are Glen's law parameters ($6.8 \times 10^{-24} \text{ Pa}^{-3} \text{ s}^{-3}$ and 3, respectively). The second term in equation 1 represents the opening of cavities due to ice sliding over a rough bed, and the third term represents creep closure of the cavity roofs. As our model does not incorporate the feedback of hydrology causing variable basal sliding, we must choose a representative value for U_b . Based on measured surface ice velocities in this area, which range between ~ 50 and $\sim 200 \text{ m y}^{-1}$ [e.g., *Colgan et al.*, 2012; *Ryser et al.*, 2014], and acknowledging that some of the motion is due to internal ice deformation, we take a representative value of 100 m y^{-1} for U_b .

The elastic sheet is included to account simplistically for the instantaneous uplift of ice, often referred to as 'hydraulic jacking' [e.g. *Röthlisberger and Iken*, 1981; *Das et al.*, 2008; *Tedesco et al.*, 2013], that we expect to occur at high water pressure. The functional form of the thickness h_{el} in *Hewitt* [2013] was taken from *Flowers and Clarke* [2002]; here we prefer a different functional form, believing that the elastic uplift we are trying to capture is more likely controlled by the effective pressure. This is the second main difference to the model set-up in *Hewitt* [2013]. Here, h_{el} depends directly on effective pressure according to the equation

$$h_{el} = C_{el} \left[-N_- + \frac{1}{2} N_0 \max \left(0, 1 - \frac{N_{\pm}}{N_0} \right)^2 \right] \quad (2)$$

157 where $N_- = \min(N, 0)$, $N_+ = \max(N, 0)$, C_{el} is an elastic compliance, and N_0 is a small regularizing
 158 pressure to make this function smooth (10^3 Pa). This function is designed to be zero for positive N
 159 but to increase rapidly when N is negative. In other words, this component of the sheet is activated
 160 when water pressure reaches or exceeds ice overburden pressure. This method of accounting for
 161 jacking is only approximate, since it does not allow for elastic bending stresses in the ice. However,
 162 the method allows for lake drainage events to be accommodated by the subglacial drainage system,
 163 without the generation of unrealistically large pressures that would occur if the water were forced
 164 into cavities and conduits. The default value for C_{el} , $1.02 \times 10^{-5} \text{ m Pa}^{-1}$, allows 1 m of uplift for each
 165 10 m of excess hydraulic head. Sensitivity tests show that the key effect of increasing C_{el} is to reduce
 166 the amplitude of the short-term (< 24 h) water pressure spikes when lakes drain; the overall water
 167 pressure trends, and drainage system development over the melt season are relatively insensitive to
 168 the precise value of C_{el} .

169 Discharge $\mathbf{q}(x, y, t)$ in the cavity sheet is given by

$$170 \quad \mathbf{q} = -\frac{K_s h^3}{\rho_w g} \nabla \phi \quad (3)$$

171 where $\phi(x, y) = \rho_w g z(x, y) + P_w(x, y)$ is the hydraulic potential, $K_s h^3$ represents an effective
 172 hydraulic transmissivity as a function of the sheet thickness (h), g is acceleration due to gravity (9.81
 173 m s^{-2}), and z is bed elevation (m).

174 Channel cross-sectional area (CSA), $S(s, t)$, with s denoting distance along a channel, evolves
 175 according to

$$176 \quad \frac{\partial S}{\partial t} = \frac{\rho_w}{\rho_i} M - \frac{2A}{n^n} S |N|^{n-1} N, \quad (4)$$

177 where M is the melt rate of the channel walls (equation 6). The final term represents creep-closure of
 178 the channel walls due to the effective pressure. The discharge in the channels is given by

$$179 \quad Q = -K_c S^{\frac{5}{4}} \left| \frac{\partial \phi}{\partial s} \right|^{-\frac{1}{2}} \frac{\partial \phi}{\partial s}, \quad (5)$$

180 where K_c is a turbulent flow coefficient ($0.1 \text{ m s}^{-1} \text{ Pa}^{-1/2}$).

181 Melting, $M(s, t)$, is given by

$$182 \quad M = \frac{1}{\rho_w L} \left| Q \frac{\partial \phi}{\partial s} \right| + \lambda \frac{|q \cdot \nabla \phi|}{\rho_w L}, \quad (6)$$

where L is the latent heat of melting (freezing point dependence on pressure is neglected here), and λ is the incipient channel width (i.e. the width scale over which basal-ice melting contributes to channel initiation; 10 m [from *Hewitt*, 2013]).

Mass conservation is expressed as

$$\frac{\partial h}{\partial t} + \nabla \cdot \mathbf{q} + \left[\frac{\partial S}{\partial t} + \frac{\partial Q}{\partial S} \right] \delta(\mathbf{x}_c) + \frac{\partial \Sigma}{\partial t} = m + M\delta(\mathbf{x}_c) + E, \quad (7)$$

where englacial storage $\Sigma(x,y,t)$ is a function of water pressure

$$\Sigma = \sigma \frac{P_w}{\rho_w g} + A_m \frac{P_w}{\rho_w g} \delta(\mathbf{x}_m) \quad (8)$$

In equations 7 and 8, σ is the englacial void fraction, A_m is moulin (a vertical, cylindrical shaft) CSA (10 m^2), and the delta functions apply along the positions for the conduits $\mathbf{x}_c(s)$ and moulins \mathbf{x}_m . The source term, $E(x,y,t)$, is exclusively from moulin point sources (section 3.2.2). The englacial water storage volume in void space and moulins, Σ , has a strong influence on both the amplitude and timing of diurnal variations; the more storage, the more damped the amplitude of the pressure variations, and the greater the delay relative to the melt signal. As a final point, we note that although the physics of the channelized component in the current model is fundamentally the same as that of *Banwell et al.* [2013], the models have been parameterized in slightly different ways.

3.1.2. Parameter Values

Results described in *Hewitt* [2013] and initial sensitivity tests undertaken in the current study show that the changing structure and morphology of the subglacial drainage system (notably, whether it is predominantly distributed or channelized, and the timing of the transition from one morphology to the other) is particularly sensitive to two key parameters: the connected englacial void fraction, σ , and the sheet flux coefficient, K_s . Therefore, we identify the most suitable values for σ and K_s as follows. We perform multiple model runs with different parameter combinations. We choose values within the ranges $1 \times 10^{-4} \leq \sigma \leq 1 \times 10^{-2}$ and $1 \times 10^{-6} \leq K_s \leq 1 \times 10^{-4} \text{ Pa}^{-1} \text{ s}^{-1}$, varying by factors of 10. This includes the order of magnitude values used by *Hewitt* [2013] and gives us nine parameter combinations in total. For each model run, we compare the modeled proglacial discharge with that measured at the Asiaq station using two objective criteria. First, we compare the total discharge volumes over the time period 12 May to 31 August 2005. Second, we analyse the match between the daily mean discharge volumes through calculation of both the Nash–Sutcliffe model efficiency coefficient and the root mean square error (RMSE).

We note, however, that the measured and modeled proglacial discharge hydrographs are not directly comparable because a series of proglacial lakes introduce a temporally-varying lag between the arrival of water at the ice margin and its arrival at the Asiaq station, which is not accounted for by the model [Banwell *et al.*, 2013]. Thus, for parameterization purposes, we direct more attention to the results of the total discharge volume comparison.

3.2 Boundary Conditions and Forcings

The full model is run from 1 September 2004 to 31 August 2005. This year was selected as it is one for which the SMB model was calibrated [Banwell *et al.*, 2012a]. However, following Banwell *et al.* [2013], results are only analyzed from 12 May 2005 to 31 August 2005, which spans the melt season. From 1 September 2004 to 11 May 2005, discharge in the subglacial drainage system is entirely due to a background basal melt rate (m) (0.024 m y^{-1}), representative of that due to geothermal and frictional heating ($m = (G + \tau_b U_b) / \rho_w L$, where geothermal heat flux $G = 0.06 \text{ W m}^{-2}$ and basal shear stress $\tau_b = 60 \text{ kPa}$, which are appropriate values for this area of Paakitsoq). By 11 May 2005, the model reaches a roughly steady-state.

3.2.1. Subglacial Domain

Since one aim of our study is to assess the key differences and similarities between the results of the modified Hewitt [2013] model discussed above and that used by Banwell *et al.* [2013], we use the subglacial domain defined previously by Banwell *et al.* [2013; their section 3.2.3] (Figure 1). In reality subglacial catchments are able to vary in size due to subglacial water pressure perturbations [cf. Lindbäck *et al.*, 2015; Chu *et al.*, 2016], but the model domain needs to be defined and fixed for the current study.

Due to the way in which the catchment was defined [Banwell *et al.* 2013], no water enters the domain across the supra- or sub-glacial boundaries. Atmospheric pressure is applied at the ice margin. Water is able to outflow from the subglacial system at any point along the ice margin; outflow points are not predefined, as they had to be in Banwell *et al.* [2013]. However, if there are multiple outflow points, all water is cumulated at each time step for calibration purposes.

3.2.2. Moulin Positions

Following Banwell *et al.* [2013], we assume that all depressions in the surface DEM potentially contain a moulin in their lowest cell, which can be activated if and when a lake in a depression drains through a simulated hydrofracture event (see section 3.3.2.). Although we realize that additional moulins, not associated with surface lakes, are likely to be present on the ice-sheet surface [e.g.,

243 *Catania et al.*, 2008; *Colgan and Steffen*, 2009; *Smith et al.*, 2015; *Yang et al.*, 2015], our assumption
244 produces a maximum moulin density of 0.20 km^{-2} , which is comparable to estimates calculated by
245 *Colgan and Steffen* [2009] ($0 - 0.88 \text{ km}^{-2}$) and *Zwally et al.* [2002] (0.20 km^{-2}) for Paakitsoq.

246 The locations of the potential moulins (black dots), overlaid onto a subglacial upstream flow
247 accumulation map, are shown in Figure 2. The moulins fall on or very close to the paths of highest
248 subglacial flow accumulation [*Shreve*, 1972], along which conduit locations were prescribed by
249 *Banwell et al.* [2013].

250 **3.3. Input Hydrographs**

251 3.3.1. Surface Routing and Lake-Filling Model

252 Input hydrographs for all depressions (and hence lakes) in the surface DEM are calculated by the
253 surface routing and lake filling (SRLF) model [*Arnold et al.*, 1998, 2014; *Arnold*, 2010; *Banwell et*
254 *al.*, 2012b, 2013], which is driven with surface runoff, simulated by the SMB model [*Banwell et al.*,
255 2012a]. Briefly, the SRLF model links a surface lake and catchment identification algorithm to a
256 flow delay algorithm, to simulate water flow over both snow-covered (assuming Darcian flow) and
257 bare ice (assuming open-channel flow). However, in order to calculate moulin input hydrographs
258 (i.e. the meltwater discharge which exits the depression through a moulin in its lowest cell once a
259 lake drains), the SRLF model is linked to a surface-lake drainage model [*Clason et al.*, 2012;
260 *Banwell et al.*, 2013; *Arnold et al.*, 2014].

261 3.3.2. Surface Lake Drainage Model

262 The surface lake drainage model uses a water-volume-based threshold to trigger lake drainage
263 events. We assume that all depressions start to fill to become lakes, but that they can begin to drain
264 directly into the subglacial drainage system through a simulated hydrofracture mechanism if the lake
265 reaches or exceeds a critical volume threshold. This threshold assumes that drainage will occur
266 through a fracture if $V = F_a \cdot H$, where V is lake volume, H is the local ice thickness beneath the lake,
267 and F_a is the map-plane fracture area. This concept is based on the idea that once a fracture has been
268 initiated, it is the availability of surface meltwater for filling the expanding fracture and offsetting
269 freezing onto the walls which is crucial in controlling crevasse propagation [*van der Veen*, 2007;
270 *Krawczynski et al.*, 2009]. Although the F_a is treated as a tunable model parameter, it is constant
271 across the model domain for a given model run; thus lakes over thicker ice have to reach a larger
272 water volume in order to drain.

273 If a lake reaches the threshold volume for drainage, all water in the lake is assumed to drain rapidly
274 through a fracture. If the critical volume threshold is not reached and the surface depression reaches

capacity, the SRLF model allows lakes to overflow into the next downstream catchment. Slow lake drainage by overflow channel-incision [cf. *Tedesco et al.*, 2013] is not accounted for. Following *Banwell et al.* [2013], and based on observations of rapid lake drainage events on the GrIS [e.g., *Das et al.*, 2008; *Doyle et al.*, 2013; *Tedesco et al.*, 2013], we add the total lake volume at the time of drainage to the subglacial drainage system over a 5-hour period (a period that the model is relatively insensitive to). Subsequently, all surface meltwater that enters the topographic depression is able to reach the subglacial system directly through the open moulin, which is assumed to exist at the lowest part of the depression for the remainder of the melt season [e.g., *Shepherd et al.*, 2009; *Bartholomew et al.*, 2010; *Catania and Neumann*, 2010].

A large F_a (and the resulting high critical volume for drainage) means that few lakes will drain during the melt season; most meltwater will be stored in lakes or will flow to the ice-sheet margin supraglacially. Any lakes that drain will deliver large volumes of water to the bed, and will do so relatively late in the melt season; thus, the duration over which subsequent surface runoff can enter the subglacial system via an open moulin will be relatively short. Conversely, a small F_a (and the resulting low critical volume for drainage) means that most lakes will drain within a few weeks of the melt season commencing, the total volume of meltwater either stored in surface lakes or routed supraglacially will be low, the water volumes delivered to the bed by lake drainage will be small, and the duration over which subsequent surface runoff can enter the subglacial system will be long.

To identify the most appropriate F_a to use together with the local ice thickness in the lake volume threshold relationship, *Banwell et al.* [2013] compared modeled and measured proglacial discharge for the same 200 km² model domain as that used here; the optimal value was 1000 m². In the current study, we first use the value $F_a = 1000$ m² to calibrate key subglacial model parameters through comparison of the modeled and measured proglacial discharge hydrographs, and then we compare the results of this model run to those from *Banwell et al.* [2013]. However, since the model used here is different, this value is no longer necessarily optimal, but there is in any case uncertainty associated with the use of a constant F_a across the model domain (several recent studies have highlighted the complexity of lake drainage). For the main part of this study we therefore experiment with a range of fracture areas, which allows us to explore how varying the density and opening time of moulins affects the behavior of the subglacial drainage system.

We consider three separate scenarios: (i) a large F_a of 2500 m² (hereafter called the ‘*low moulin density scenario*’); (ii) a small F_a of 250 m² (hereafter called the ‘*high moulin density scenario*’); and (iii) a F_a of zero (hereafter called the ‘*maximum moulin density scenario*’). The third scenario effectively prevents lakes from filling, effectively assuming that all surface depressions contain

moulins, which are always open. Although allowing no lakes to fill is unrealistic, this scenario allows for the maximum possible volume of surface meltwater delivery to the bed, with no delay due to surface storage in lakes.

4. Results and Analysis

4.1. Calibration of Key Parameters

The difference between total cumulative volumes of modeled (ΣMo) and measured (ΣMe) proglacial discharge varies significantly (-15 to 4% of ΣMe) for different combinations of parameter values for the connected englacial void fraction (σ) and the sheet flux coefficient (K_s) (Table 1). The minimum difference between ΣMo and ΣMe discharge is produced with the values $\sigma = 1 \times 10^{-4}$ and $K_s = 1 \times 10^{-5} \text{ Pa}^{-1} \text{ s}^{-1}$, which also give a relatively low RMSE and a relatively high Nash Sutcliffe coefficient. However, in terms of the lowest RMSE and highest Nash Sutcliffe coefficient, the best match between the modeled and measured discharge hydrographs is produced with the values $\sigma = 1 \times 10^{-3}$ and $K_s = 1 \times 10^{-4} \text{ Pa}^{-1} \text{ s}^{-1}$, although for these values, the difference between ΣMo and ΣMe discharge is higher. As minimizing the difference between ΣMo and ΣMe discharge is considered to be the best parameterization method (section 3.1.2.), we use the parameter values $\sigma = 1 \times 10^{-4}$ and $K_s = 1 \times 10^{-5} \text{ Pa}^{-1} \text{ s}^{-1}$ for the remainder of this study.

It is encouraging that the modeled proglacial discharge hydrograph using these chosen parameter values produces a closer statistical match with the measured proglacial discharge data (Table 1) than that found by *Banwell et al.* [2013] (their ΣMo minus $\Sigma Me = 1.7 \times 10^7 \text{ m}^3$, RMSE = $25.8 \text{ m}^3 \text{ s}^{-1}$, Nash Sutcliffe coefficient = 0.45, compared to our values of $2.4 \times 10^6 \text{ m}^3$, $19.7 \text{ m}^3 \text{ s}^{-1}$ and 0.68, respectively).

4.2. Comparison of the Two Models

Under the assumption that $F_a = 1000 \text{ m}^2$, we analyze the modeled water pressure in the same eight moulins that were shown in *Banwell et al.* [2013; their Figure 5] (Figure 3; see Figure 2 for moulin/lake locations, and Table 2 for lake drainage dates). To enable water pressures to be compared to the results from *Banwell et al.* [2013], and also across the model domain, we express water pressure as a fraction of ice overburden pressure, i.e., P_w/P_i . The input hydrographs for the 9 moulins that open-up for this scenario are shown in Figure S1.

In general, there are strong similarities between the time series of modeled pressures from the two models (Figure 3). Both produce a general transition from relatively high average subglacial water pressure with low amplitude diurnal cycles, to lower average pressure and higher amplitude cycles, as the melt season progresses; this change is indicative of increasing hydraulic efficiency (i.e.

channelization) within the subglacial system [e.g., Bartholomew *et al.*, 2010; Colgan *et al.*, 2012; Chandler *et al.*, 2013; Cowton *et al.*, 2013] (see also Figure S2, and section 5.2 for further discussion). Furthermore, lake drainage events in both studies cause short-term rapid increases in subglacial water pressure up to, or above, ice overburden pressure (i.e. $P_w/P_i \geq 1$). However, there are five key differences between the model results:

- i) Pressure spikes due to lake drainage events in the current study reach a maximum of $P_w/P_i \approx 1.3$, the magnitude of which is controlled by the elastic compliance (C_{el}) of the elastic sheet (Figure 3) (e.g. Setting C_{el} to half its current value generates spikes in $P_w/P_i \leq 1.5$). In contrast, pressure spikes in the study by Banwell *et al.* [2013] were capped at $P_w/P_i = 1.1$, as water at this threshold pressure overflowed from moulins and onto the ice-sheet surface;
- ii) In the current study, the early melt season water pressure across the domain is relatively high ($P_w/P_i \approx 0.7$), and following pressure spikes due to lake drainage events, pressures tend to remain high (i.e. $P_w/P_i \approx 1$) for up to 7 days. In contrast, Banwell *et al.* [2013] found much lower early melt season water pressures ($P_w/P_i \approx 0$), and the return of pressures to $P_w/P_i < 0.5$ within two to three days of a rapid drainage event (e.g. compare plots for Moulins 582 and 444, where lakes drained on 21 May and 12 June, respectively; Figure 3a).
- iii) Lake drainage events in the current study substantially increase subglacial water pressures within a very localized area (< 1 km). Conversely, Banwell *et al.* [2013] found that lake drainage events caused concurrent high-pressure spikes ($P_w/P_i \geq 1$) up to ~ 5 km from the location of the drained lake. For example, in that study, the drainage of Lake 551 on 1 June caused a pressure spike in Moulin 572 (despite Lake 572 not draining until 10 June) (Figure 3a), and the drainage of Lake 444 caused a pressure spike in Moulin 468. This phenomenon is not seen in the current study (Figure 3b);
- iv) The timing of the drop to lower average pressures, and of the emergence of higher-amplitude diurnal cycles (i.e. indicative of a switch from an inefficient system to more efficient channels), generally occurs later in the current study than in that by Banwell *et al.* [2013], particularly for the moulins furthest inland. For example, Moulins 468 and 494 (the highest-elevation moulins to open), show diurnally varying pressure from early-mid August and mid-late July, respectively, whereas Banwell *et al.* [2013] observed diurnal variations in these moulins from mid-June and early July, respectively (Figure 3b). Meanwhile, Moulin 572 (at a lower elevation, ~ 15 km from the ice margin), shows diurnally varying water pressure from early July, compared to from mid-June in Banwell *et al.* [2013]. However, diurnally varying

water pressure in Moulin 582 (also ~15 km from the ice margin) is observed from mid-June in both models;

- v) Diurnal variations in subglacial water pressure (as seen in many moulins from 1 July) in the current study are generally lower in amplitude than those found by *Banwell et al.* [2013] (Figure 3b).

Excluding point (i), the likely reason for the differences between the two sets of modeled water pressures summarized in points (ii) – (v) is that the current subglacial routing model includes both a distributed and channelized system, whereas that used by *Banwell et al.* [2013] was composed solely of channels. Regarding point (ii) in particular, although the channels in *Banwell et al.* [2013] could enlarge through wall melting during the melt season, thus increasing their efficiency, their relatively low capacity in the early melt season (minimum CSA = 0.07 m²) was greater than the capacity of the early-season distributed system in the current study. The current study also has a background basal melt rate, which did not exist in the *Banwell et al.* [2013] study.

Regarding point (iii), in the current study, lake drainage events result in rapid rises in water pressure within a localized region (< 1 km), followed by relatively sustained high-pressure ($P_w/P_i \approx 1.0$) due to the accommodation of water in the surrounding distributed system. In contrast, lake drainage events in the *Banwell et al.* [2013] study caused immediate pressure spikes in the subglacial channels and moulins connected to them up to ~5 km from the draining lake, but pressures quickly fell back to near-atmospheric levels as the channels rapidly routed the water away.

Regarding point (iv), the later occurrence of higher-amplitude diurnal cycles in water pressure in the current study, which is indicative of a later onset of channelization, is also due to the presence of a distributed system and the lack of a predefined channel network. In the current study, water initially flows in many directions and its dissipative melting of the ice is not concentrated along any specific pathway, thus channels develop relatively slowly and high water pressure is maintained for a relatively long time. In contrast, water in the *Banwell et al.* [2013] model was forced to follow channels that had prescribed locations and a minimum CSA; dissipative heating from water flow was focussed on widening those routes, allowing conduits to enlarge more quickly than in the current study, and thus enabling water pressures to drop more quickly. Although the first scenario seems a priori more realistic, the latter scenario may better represent reality if preferred subglacial pathways are maintained through the winter [e.g. *Gulley et al.*, 2012], which might be possible under the relatively thin ice of the GrIS margins.

Regarding point (v), the lower amplitude diurnal water pressure variations in the current study are because the pressure is moderated by the ability of water to exchange between the distributed and channelized systems. At times of high surface meltwater inflow (e.g. in the afternoon), the channels pressurize, forcing water into the distributed system, whereas when the surface water inflow reduces (e.g. at night), water will flow out of the distributed system and into the channels [e.g., *Hubbard et al.*, 1995]. Conversely, in the channel-only model of *Banwell et al.* [2013], the channels were likely at high pressure during the day, and at atmospheric pressure during the night.

4.3. Model Sensitivity to Moulin Density

For the low moulin density scenario (i.e. $F_a = 2500 \text{ m}^2$), five lakes drain rapidly during the melt season (and thus, five moulins open, giving a moulin density of 0.02 km^{-2}), the mean lake volume at the time of drainage is $1.0 \times 10^6 \text{ m}^3$, and the mean drainage date is 12 June (Table 2). For the ‘optimum’ scenario (i.e. $F_a = 1000 \text{ m}^2$, from *Banwell et al.*, 2013], 9 lakes drain rapidly during the season (i.e. 9 moulins open, moulin density = 0.05 km^{-2}), the mean lake volume at the time of drainage is $4.1 \times 10^5 \text{ m}^3$, and the mean drainage date is 4 June. For the high moulin density scenario (i.e. $F_a = 250 \text{ m}^2$), 18 lakes drain rapidly (i.e. 18 moulins open, moulin density = 0.08 km^{-2}), the mean water volume at the time of drainage is smaller ($9.6 \times 10^4 \text{ m}^3$), and the mean drainage date is earlier (24 May). For the maximum moulin density scenario (i.e. $F_a = 0 \text{ m}^2$), all 40 moulins are open for the duration of the model run (density = 0.20 km^{-2}).

The proportion of fast draining lakes, as a percentage of the total number of surface lakes in the model domain (40), is 13% and 45% for the low and high moulin density scenarios respectively. Thus, these two moulin density scenarios likely span the realistic range of lake-bottom moulin input distributions given that the lower of these values (13%) is comparable to the percentages of observed fast-draining lakes across the entire GrIS [13%; *Sundal et al.*, 2011], and for South-West Greenland [14%; *Selmes et al.*, 2013].

In the following three sections, we discuss further the results for the low, high and maximum moulin density scenarios. For comparison, the results for the ‘optimum’ moulin density scenario are also shown in Figure S2; they are intermediate between the low and high moulin density scenarios.

4.3.1. Low Moulin Density Scenario

Lake drainage events in the low moulin density scenario occur at higher elevations as the melt season progresses, and produce localized zones of high discharge and water pressure, which subsequently move down-glacier (Figure 4a; Movies S1 and S2). For example, following the drainages of Lake 444 on 18 June (Figure 4a, 28 June), and then Lake 468 on 4 July (Figure 4a, 14

July), high pressure waves steadily move down-glacier over the remaining melt season (Figure 4a, 30 July – 31 August). Such pronounced pressure waves develop when a sudden pulse of meltwater is received by an area of the subglacial system that has previously experienced few (or no) large meltwater pulses associated with lake drainage events, and little (or no) subsequent surface meltwater inputs via an open moulin.

Thus, for the low moulin density scenario, the lack of an already-developed channelized system means that water from a drained lake cannot easily be accommodated, or routed efficiently, by the drainage system, which is still largely distributed. It is relatively hard for water from a lake drainage event to initiate channel formation, despite the relatively large water volumes involved [e.g., *Dow et al.*, 2014]. Additionally, as the lakes drain relatively late in the season, there is little time remaining for surface meltwater to enter the subglacial system to help develop and sustain a channel once it has been initiated. Therefore, by the end of the season, the bulk of the meltwater is still flowing in the cavity sheet, while some is carried by a few poorly-developed channels covering a small proportion of the domain (Figure 4a, 31 August).

For the melt season as a whole, the mean water pressure for the low moulin density scenario is highest up-glacier and in the more southerly regions of the domain, and lowest in the ice-marginal and more northerly regions (Figure 5a). Additionally, there are three central areas that have a lower mean water pressure ($P_w/P_i \sim 0.45$) than their neighboring areas ($P_w/P_i \sim 0.75$), suggesting that channels have grown to a large size as water fluxes are concentrated there.

It is more informative, however, to look at patterns of water pressure and its variability through the melt season, as it is these that have important implications for basal sliding [e.g., *Pimentel and Flowers*, 2010; *Schoof*, 2010; *Colgan et al.*, 2012]. For the low density moulin scenario, large areas of the bed experience high, sustained pressures for many days (Figure 6a), due to the dominance of a distributed system during the melt season. For example, 18% of the subglacial domain experiences high water pressures (i.e. $P_w/P_i \geq 1$) for five days or more, while 8% of the domain experiences $P_w/P_i \geq 1$ for 10 days or more. The lack of channels means that diurnal variations in water pressure are generally low in amplitude over the majority of the bed (Figure 6b); only 6% of the domain experiences a diurnal range in $P_w/P_i \geq 0.2$ for 30 days or more, while only 0.4% of the domain experiences a diurnal P_w/P_i range ≥ 0.2 for 50 days or more. The area where pronounced diurnal water pressure fluctuations occur for the longest time is in the north of the domain, where channels first develop.

4.3.2. High Moulin Density Scenario

467 The high moulin density scenario means that lakes drain relatively early in the melt season such that
468 when a particular lake drains, there is a high likelihood that at least one nearby lake (probably down-
469 glacier) has already drained. As previous lake drainage events, followed by subsequent moulin water
470 inputs, will have increased the efficiency of the major conduits (at least over some areas of the bed),
471 additional pulses of meltwater to the subglacial system will be accommodated and routed more
472 easily. Thus, large areas of high water pressures, with pressure waves travelling down-glacier, do not
473 dominate (Figure 4b; Movie S4), in contrast to the results for a low moulin density (Figure 4a;
474 Movie S2). Instead, for a high moulin density, we see initially highly fluctuating water pressures
475 (corresponding to diurnal fluctuations in surface meltwater inputs) in localized areas around the
476 numerous moulins that are receiving meltwater after the lakes have drained (e.g. as indicated by the
477 rapidly shifting hydraulic potential contours in Movie S3, and the highly variable P_w/P_i in Movie S4).
478 Such localized areas of highly fluctuating water pressures advance up-glacier through the melt
479 season as lakes at higher elevations drain, and their amplitude decreases as conduits become more
480 efficient and meltwater is more efficiently routed away from the moulins (Figure 4b, 28 June – 31
481 August).

482 By the end of the melt season, a denser network of well-developed channels exists with only a small
483 proportion of water accommodated by the cavity sheet (Figure 4b, 31 August; Movie S3), in contrast
484 to the low density moulin results (Figure 4a, 31 August; Movie S1). We note that the positions of
485 these main drainage pathways, as well as the main marginal outlet, are very similar to those that were
486 assumed (and fixed for that model run) by *Banwell et al.* [2013; their Figure 2].

487 Over the entire melt season, the mean water pressure for the high moulin density scenario (Figure 5b;
488 overall mean $P_w/P_i = 0.613$ (std dev = 0.255)) is very similar to that for the low density moulin
489 scenario (Figure 5a; overall mean $P_w/P_i = 0.625$ (std dev = 0.254)), which can be expected, given that
490 low pressure channels take up little space relative to the higher pressure distributed system.
491 However, there are some key differences in the season mean water pressures between the two
492 scenarios (Figure 5c). Whereas the high moulin density scenario results in lower mean pressures in
493 the ice-marginal/down-glacier region of the domain (i.e. the red/orange areas, Figure 5c), this
494 scenario also results in higher mean pressures in some of the more up-glacier regions of the domain
495 (i.e. the blue areas, Figure 5c). Thus, opening additional moulins leads to reduced mean water
496 pressures in some areas, as there is sufficient water flux and/or time for channelization to occur,
497 which lowers water pressure. However, in other areas, opening additional moulins results in higher
498 mean water pressures, as there is insufficient water flux and/or time for channelization to occur, and
499 thus the distributed system pressurizes further.

500 In terms of intra-seasonal water pressure patterns for the high moulin density scenario, only small
501 areas of the bed experience multi-day periods of high water pressures. For example, only 9% of the
502 bed experiences $P_w/P_i \geq 1$ for five days or more, and only 5% of the bed experiences $P_w/P_i \geq 1$ for ten
503 days or more (Figure 6c). This is due to the relatively rapid growth of efficient channels across a
504 large portion of the bed from early in the melt season (Figure 4b, Movies S3 and S4), which also
505 explains why high-magnitude, and widespread, diurnal fluctuations in pressure are seen for a
506 significant proportion of the melt season. For example, 20% of the bed experiences a diurnal range in
507 $P_w/P_i \geq 0.2$ for 30 days or more, while 10% of the bed experiences a diurnal range in $P_w/P_i \geq 0.2$ for
508 50 days or more (Figure 6d). Additionally, 1% of the domain experiences a diurnal range in $P_w/P_i \geq$
509 0.2 for 70 days or more, and these areas appear as ‘ribbons’ (i.e. the red areas, Figure 6d), where
510 channelization is most pronounced.

511 4.3.3. Maximum Moulin Density Scenario

512 The development of the subglacial drainage system for the maximum moulin density follows a
513 similar pattern as for the high moulin density scenario, although channelization occurs from even
514 earlier in the melt season and results in an even denser end-of-season channel network (Figure S3,
515 Movies S5 and S6). This is a consequence of all 40 moulins being open at the start of the season;
516 lakes do not fill and drain, and all surface meltwater is routed to the bed as soon as it reaches the
517 lowest cell in a topographic depression, with minimal surface water storage.

518 The mean seasonal water pressure across the domain (Figure S4a; overall mean $P_w/P_i = 0.616$ (std
519 dev = 0.261)) is again similar to that for the low and high moulin density scenarios (Figures 6a and
520 b, respectively), although the key differences between the low and maximum moulin density
521 scenarios (as outlined above) are even greater (Figure S4b). Regarding intra-seasonal water pressure
522 variations, more areas of the bed experience sustained periods of high water pressures for the
523 maximum moulin density scenario (Figure S3), but these areas are smaller than for the high moulin
524 density scenario (Figure 4b). Thus, the proportions of the domain that experiences $P_w/P_i \geq 1$ for 5 and
525 10 days (or more) are actually identical to those for the high moulin density scenario (9% and 5%,
526 respectively) (Figure 6e). However, compared to the high moulin density scenario, the maximum
527 moulin density scenario experiences high-magnitude, diurnal water pressure fluctuations that are
528 even more widespread and last for longer. For example, 34% of the bed experiences a diurnal range
529 in $P_w/P_i \geq 0.2$ for 30 days or more, and 15% of the bed experiences a diurnal range in $P_w/P_i \geq 0.2$ for
530 50 days or more (Figure 6f).

531 However, for the maximum moulin density scenario, the proportion of the bed that experiences a
532 diurnal range in $P_w/P_i \geq 0.2$ for 70 days or more (i.e. the red areas, Figure 6f) is $< 1\%$, which is
533 actually slightly less than that for the high moulin density scenario (Figure 6d). This is indicative of a
534 slightly different pattern of conduit development; although numerous channels are initiated as a
535 result of the more spatially distributed surface meltwater inputs, individual channels do not develop
536 as much as they did for the high moulin density scenario because meltwater inputs are less focused
537 into specific areas of the bed. In contrast, the high density moulin run receives more focused inputs
538 (i.e. not all moulins open, and thus some surface depressions fill to form lakes, then overflow into
539 other lakes down-glacier, contributing to their volume and/or moulin inputs).

540 **5. Discussion**

541 **5.1. Comparison of the Two Models with Field-Based Studies**

542 In general, strong similarities are seen between the time-series of modeled subglacial water pressures
543 from this study and those from *Banwell et al.* [2013], giving us confidence that the inferences drawn
544 from previous channel-only modeling studies for Paakitsoq [*Banwell et al.*, 2013; *Mayaud et al.*,
545 2014] are robust; the earlier simple model captures key aspects of the system behaviour observed in
546 the current, more complex, model. As both studies have identical inputs and boundary conditions,
547 the five main differences that we observe (section 4.2.) are due solely to the different representations
548 of the subglacial hydrology; most importantly, the presence of a distributed system in the current
549 model compared to the channel-only model of *Banwell et al.* [2013].

550 In comparison to the Asiaq measured proglacial discharge data, the current model produces a closer
551 statistical match than that found by *Banwell et al.* [2013] (section 4.1). However, as we have no other
552 field-based hydrology data for the precise region in 2005 (e.g. moulin/borehole water levels or
553 englacial/subglacial water velocities from tracing experiments), and as our models do not predict
554 basal sliding rates (which could be compared to field- or satellite-derived ice velocity data) it is hard
555 to validate the models to establish which one gives a better representation of reality. However, in the
556 following two sub-sections, we compare our results with field-based measurements of i)
557 moulin/borehole water levels; ii) water velocities from tracing experiments; and iii) ice velocities, all
558 from other marginal regions of the GrIS, and/or from different years.

559 **5.1.1. Comparison with Moulin/Borehole Pressure Measurements**

560 With reference to measured borehole pressure data from marginal regions of the GrIS [e.g. *Luthi et*
561 *al.* 2002; *Andrews et al.*, 2014; *Wright et al.* 2016], we suggest that the higher early-season water
562 pressure found by the current study (i.e. $P_w/P_i \approx 0.7$ before any lake drainage events, cf. $P_w/P_i \approx 0$ in

563 *Banwell et al.* [2013]) is the more realistic of the two set of model results. Additionally, diurnally-
564 fluctuating borehole water pressures from marginal regions (<30 km inland) of the GrIS have been
565 measured at $0.76 \geq P_w/P_i < 1.17$ [*Andrews et al.* 2014; *Van de Wal et al.* 2015; *Wright et al.* 2016],
566 suggesting that the mid- to late-season lower amplitude cycles found in the current model are more
567 realistic than those found by *Banwell et al.* [2013]. Finally, *Wright et al.* [2016] first observed
568 diurnally varying, and a drop to lower average, borehole water-pressures (measured 27 km inland
569 from Isunnguata Sermia, west Greenland) in late June 2011 and 2012, which is more in line with the
570 results of the current model.

571 5.1.2. Comparison with Tracing Experiment Results

572 *Cowton et al.* [2013] and *Chandler et al.* [2013] used dye-trace data to infer that a degree of
573 channelization had occurred in the lower 14 km of Leverett Glacier, West Greenland, by late
574 May/early June 2010. This is two weeks earlier than when the channel-only model of *Banwell et al.*
575 [2013] saw signs of a significant increase in channel efficiency ~ 15 km from the ice margin, and
576 closer to four weeks earlier than when the current model starts to show signs of channelization (e.g.
577 cf. Moulins 551 and 572, Figure. 3a).

578 5.1.3 Comparison with Ice-Velocity Measurements

579 In contrast to the results of *Cowton et al.* [2013] and *Chandler et al.* [2013], *Hoffman et al.* [2011]
580 observed a sustained (> 40 days) increase in surface ice motion ($> 50\%$ above winter background)
581 from mid- to late June in 2007 in the area around JAR1 in the Paakitsoq region, suggesting that
582 widespread channelization did not occur until mid- to late July. Likewise, *Ryser et al.* [2014] did not
583 observe any significant increases in ice velocity at FOXX (~ 20 km inland from the ice margin at
584 Paakitsoq) until early to mid-June in 2012, again suggesting that channelization did not occur in this
585 region for at least a few weeks after this. Thus, ice velocity measurements from Paakitsoq, but from
586 other years, appear to be more in line with the results of the current study.

587 5.1.4 Comparison Summary

588 The current model, which includes both distributed and channelized drainage components, appears to
589 better match previous studies of borehole water-pressures and ice velocities, in terms of the
590 magnitude and timing of water pressure fluctuations and the onset of channelization to mid- to late
591 June, than the channel-only model of *Banwell et al.* [2013]. In contrast, the timing of the onset of
592 channelization inferred from tracer experiments appears to be better matched in the channel-only
593 model than the current model, although it still occurs about two weeks earlier than the channel-only

594 model predicts.

595 Possible reasons for the delay of channel initialization in our current model compared to that inferred
596 by *Cowton et al.* [2013] and *Chandler et al.* [2013] are: i) an over-prediction of conduit creep-
597 closure rates during low discharge; ii) the localized uplift mechanism during over-pressured periods
598 not fully accounting for the non-local effects of hydraulic jacking away from the moulins; and iii)
599 not accounting for the role of sediment erosion in conduit enlargement. However, the earlier
600 channelization inferred by *Cowton et al.* [2013] and *Chandler et al.* [2013] is also likely to be
601 because 2010 was a particularly intense melt year [e.g. *van As et al.* 2012].

602 **5.2. Effect of Moulin Density on Subglacial Drainage Development**

603 Our results show that there is a gradual up-glacier transition from an inefficient (distributed) to an
604 efficient (channelized) system through the melt season for all moulin density scenarios (Figures 3, 4,
605 S2 and S3; Movies S1, S3 and S5). This progression follows an increase in the magnitude and
606 variability of meltwater inputs to the bed, which is due to increased melt rates and decreased
607 refreezing and storage in the snowpack [cf., *Bartholomew et al.*, 2010; *Colgan et al.*, 2012; *Chandler*
608 *et al.*, 2013; *Cowton et al.*, 2013]. In effect, the growth of a channelized system follows the up-
609 glacier development of surface drainage, and advances in a stepwise manner as more moulins open
610 at progressively higher elevations over the melt season, similar to the situation that has been reported
611 from valley glaciers [*Nienow et al.*, 1998; *Willis et al.*, 2002]. This general up-glacier progression of
612 lake drainage events and moulin activation occurs because at lower elevations: (i) surface melting
613 commences earlier; (ii) melt rates are higher; and (iii) ice is generally thinner, meaning that lakes do
614 not need to fill to such a large volume before they drain as they would for thicker ice at higher
615 elevations [*McMillan et al.*, 2007; *Sundal et al.*, 2011; *Banwell et al.*, 2013; *Arnold et al.*, 2014].

616 However, as shown by the contrasting results of model runs with low, high and maximum moulin
617 densities (Figures 4, S3 and 5), the timing of channel initialization and the final extent of
618 channelization across the bed are also strongly controlled by the opening time and overall density of
619 moulins that develops during the melt season. For the low moulin density scenario, few lakes drain,
620 they do so relatively late in the season, the onset of channelization is relatively late, and just a few
621 well-developed channels exist by the end of the season (Figure 4a). In contrast, for the high moulin
622 density scenario, many more lakes drain, they do so earlier in the season, thus the onset of
623 channelization is earlier, and by the end of the season, a denser network of channels exists over a
624 larger proportion of the bed (Figure 4b).

625 Superimposed on the general trend of a seasonal increase in subglacial drainage efficiency, for all
626 moulin density scenarios, are three distinctive phenomena: i) water pressure spikes (i.e. where P_w/P_i
627 ≥ 1 for < 24 h); ii) sustained high pressure periods (i.e. where $P_w/P_i \geq 1$ for > 5 days); and iii) high-
628 amplitude diurnal variations in water pressure (i.e. where $P_w/P_i \leq 0.2$ and ≥ 0.8). Pressure spikes are
629 generally caused by the rapid inflow of large water volumes at the time of lake drainage events
630 (Figure 3a), which have also been observed in subglacial pressure borehole data [e.g. *Luthi et al.*,
631 2002]. Unsurprisingly, our results suggest that more spikes in water pressure are produced when the
632 density of moulins is higher, because these moulins open due to rapid lake drainage events.

633 Periods of sustained high pressure are generally observed immediately after, and in areas down-
634 glacier from, lake drainage events (Figures 3b, 4, S2, S3, 5a, c and e), consistent with other field- and
635 modeling-based studies [*Pimentel and Flowers*, 2010; *Hoffman et al.*, 2011; *Palmer et al.*, 2011;
636 *Banwell et al.*, 2013; *Dow et al.*, 2015]. This is because high volumes of surface meltwater continue
637 to enter the distributed drainage system after the initial drainage event, causing the system to exhibit
638 a positive relationship between water discharge and pressure until channels have had time to develop
639 [*Spring and Hutter*, 1981; *Pimentel and Flowers*, 2010; *Schoof*, 2010]. However, if the discharge and
640 pressure gradient are not sufficient to initiate channelization, waves of high sustained pressure will
641 move down-glacier, as observed following the drainage of Lakes 444 and 468 for instance (section
642 4.3.1). This indicates the importance of a turbulent sheet for enabling water to move readily at the
643 ice-bed interface in the absence of extensive channelization [e.g. *Dow et al.* 2014]. Compared to the
644 higher moulin density scenario, which causes a greater rate of channelization across the bed (Figure
645 4b and Movie S4), such pressure waves are more prevalent in the low moulin density scenario due to
646 the relatively slow development of a channelized system (Figure 4a and Movie S2).

647 Large diurnal variations in P_w/P_i occur mid- to late melt season (Figures 3, 4, S2, S3, 5b, d and f).
648 These have also been observed in field-derived borehole data from western Greenland [*Thomsen et al.*
649 *et al.*, 1991; *Cowton et al.*, 2013; *Meierbachtol et al.*, 2014; *Andrews et al.*, 2014; *Ryser et al.*, 2014;
650 *Doyle et al.*, 2015; *van de Wal et al.*, 2015; *Wright et al.* 2016], and are due to the pressurization of
651 already-developed channels that are unable to enlarge fast enough to accommodate the surface-
652 derived meltwater pulse. This is in support of the finding that the variability rather than magnitude of
653 meltwater inflow has the greatest impact on water pressures [e.g., *Schoof*, 2010; *Colgan et al.*, 2011;
654 *Bartholomew et al.*, 2012]. In the present study, the large diurnal P_w/P_i variations coincide with times
655 of high diurnal variability in moulin inputs, and occur in areas where channels have become most
656 developed. Thus, a higher density of moulins results in longer time periods where large diurnal
657 variations in P_w/P_i prevail, which persist over a larger area of the bed.

658 *Banwell et al.* [2013] fixed their subglacial conduit locations under the assumption that $P_w/P_i =$
659 0.925, which was based on the theory that major drainage pathways are created when P_w/P_i is close
660 to/at ice-overburden pressure, but then remain in similar positions once water pressures drop, since
661 they are unable to migrate laterally to areas of the bed with a lower hydraulic potential [e.g., *Sharp et*
662 *al.*, 1993; *Hubbard et al.*, 1995]. The current study confirms that this was a reasonable assumption as
663 our results (particularly for the higher moulin density scenarios) suggest that the overall drainage
664 network structure is not only relatively static during the melt season (Figure 4b), but that the end-of-
665 season drainage network (Figure 4b, 31 August) is also very similar to that prescribed by *Banwell et*
666 *al.* [2013; their Figure 2].

667 **5.3. Implications of Moulin Density for Sliding**

668 Although our subglacial routing model is not coupled to a sliding model, it is possible to infer where
669 and when enhanced basal sliding is likely to occur by analyzing our modeled spatial and temporal
670 patterns of P_w/P_i in the context of results from other model- and field-based studies. Such studies
671 have indicated that the three distinct water pressure phenomena discussed earlier (section 5.2), have
672 implications for basal sliding, and thus ice velocity. First, water pressure spikes due to lake drainage
673 events may cause or prolong short-term ice uplift and speedup in the early to mid- melt season [e.g.,
674 *Das et al.*, 2008; *Van de Wal et al.*, 2008, 2015; *Pimentel and Flowers*, 2010; *Doyle et al.*, 2013;
675 *Tedesco et al.*, 2013; *Ryser et al.*, 2014; *Stevens et al.* 2015]. Our results suggest that a high moulin
676 density would lead to greater, and more widespread, short-term velocity increases during the early to
677 mid-melt season, because more water pressure spikes occur due to more lake drainage events. This
678 result, however, is directly related to how we prescribe our moulins to open.

679 Second, sustained high water pressure during the early to mid- melt season has been inferred from
680 measurements of longer-term velocity increases of marginal areas of the GrIS during the so-called
681 ‘summer regime’ [*Joughin et al.*, 2008; *Shepherd et al.*, 2009; *Bartholomew et al.*, 2010; *Hoffman et*
682 *al.*, 2011; *Palmer et al.*, 2011; *Colgan et al.*, 2012; *Ryser et al.*, 2014]. Compared to a high moulin
683 density, our results suggest that a lower moulin density results in more localized channel
684 development from relatively late in the season, causing more sustained high water pressures; this
685 would provide a greater potential for a more sustained and widespread ice velocity increase.

686 Third, large, short-term (typically diurnal) variations in water pressure in the later part of the melt
687 season have been shown theoretically to generate short-term high-velocity events, even once the
688 drainage system is predominantly channelized [*Pimentel and Flowers*, 2010; *Schoof*, 2010]. Such
689 high-velocity events have also been observed in field-based studies on the GrIS in the mid- to late

690 season [Shepherd *et al.*, 2009; Hoffman *et al.*, 2011; Bartholomew *et al.*, 2012; Cowton *et al.*, 2013;
691 Andrews *et al.*, 2014; Ryser *et al.*, 2014]. As our results suggest that a higher moulin density leads to
692 more widespread channelization from earlier in the season, which leads to larger areas of the bed
693 exhibiting high diurnal water-pressure variations, a higher moulin density may result in a higher
694 prevalence of short-term late season high-velocity events, compared to a lower moulin density.

695 However, the picture that is emerging in terms of the overall impact of drainage system evolution on
696 ice velocity is very complex. Early to mid-season channelization, which we suggest may be
697 correlated with a higher moulin density, leads to a gradual reduction in average water pressures and
698 ice velocities over that time [e.g., Sundal *et al.*, 2011; Bartholomew *et al.*, 2012; Cowton *et al.*, 2013;
699 Tedstone *et al.*, 2015]. However, early channelization may also cause greater fluctuations in water
700 pressures later in the season, and this may lead to higher average late-season ice velocities. The
701 extent to which short-term increases in late season velocity may counteract the reduced early to mid-
702 season velocities requires further study.

703 Additionally, over annual and decadal timescales, the impact of spatially- and temporally-variable
704 surface melting and water delivery to the bed on velocities requires further study. Recent work
705 suggests that for marginal areas of the GrIS, increased surface melting produces faster ice motion
706 during summer, but slower movement over the following winter, as a result of the growth of an
707 efficient drainage system that allows more water to drain from larger areas of the ice-sheet bed with
708 a high basal water pressure [Sole *et al.*, 2013; Tedstone *et al.*, 2013]. Furthermore, there appears to
709 be a cumulative effect, with successive years of high surface melting causing a year-on-year increase
710 in the extent of channelization across the bed, and an overall reduction in annual velocities, at least
711 for land-terminating regions with ice thicknesses $< \sim 1,100$ m [Tedstone *et al.*, 2015].

712 The results of this study show is that it is not only the volume and areal extent of surface melt that is
713 important in driving subglacial drainage development, water pressures and therefore ice velocities,
714 but also areal moulin density; how many moulins open, and when and where they open. If moulin
715 density varies from year-to-year, so too will the timing of channel initialization and the peak extent
716 of channelization across the bed. Therefore, the effects of this on water pressures and ice motion will
717 be combined with any changes in water pressures or ice motion due to increased melt rates.

718 **5.4. Model Limitations**

719 This study has employed a surface-lake drainage model, which uses a water-volume-based threshold
720 equal to a prescribed fracture area (a tunable parameter) multiplied by the local ice thickness, to
721 simulate lake drainage events (and thus moulin opening). The way in which the subglacial drainage

system evolves, and the resultant spatial and temporal patterns of water flux and pressures, are very sensitive to the value of this parameter, which controls the pattern and timing of water delivery to the bed. It is for this reason that the primary aim of this study involves the use of a variety of fracture areas, to create low, high and maximum moulin density scenarios.

To better understand the basal conditions beneath the GrIS, more research is required into the precise fracture mechanism and the factors that influence it [e.g. *Stevens et al.*, 2015]. Similarly, there is a need to establish the importance of fractures outside of lake basins in capturing water and delivering it to the bed. Such research will enable a more accurate prediction of water delivery to the ice-sheet bed, including lake drainage events, over space and through time.

Finally, to calculate and to predict changes in ice dynamics of marginal regions of the GrIS, this or similar models should be coupled to a sliding model [e.g. *Hewitt*, 2013] and forced with real boundary conditions and water inputs. Ideally, such a model should be constrained with field-derived data such as borehole water pressures and surface ice velocities, to better establish how moulin density affects ice dynamics over intra- and inter-seasonal timescales. Once this has been established for the past, such a model could be used to examine future ice-sheet hydrology and dynamics. The need for such research is becoming increasingly important as future melt rates are predicted to rise [e.g., *Hanna et al.*, 2013], which could lead to earlier lake drainage events (and thus earlier moulin opening times) at lower elevations [e.g., *Mayaud et al.*, 2013], and possibly higher-elevation lake drainage events [cf., *Leeson et al.*, 2014; *Poinar et al.*, 2015] (thus higher-elevation moulin openings).

6. Conclusions

We have developed and applied a high spatial (200 m) and temporal (1 h) resolution subglacial hydrological model to a ~200 km² land-terminating, ablation area of Paakitsoq, West Greenland, for the 2005 melt season. The subglacial model, which is based on that of *Hewitt* [2013], has both distributed and channelized components, and has been adapted for use with both the real topographic boundary conditions and the calibrated, modeled moulin inputs from *Banwell et al.* [2013].

Using the optimum moulin density established by the earlier study of *Banwell et al.* [2013]), we find strong similarities between the time-series of modeled subglacial water pressures from this study and those from *Banwell et al.* [2013], particularly in the mid- to late melt season when large areas of the bed have become channelized. Compared with the earlier study, we find a more complex set of behaviors, and an improved fit with the observed proglacial discharge data; differences that are

attributed to the presence of a distributed system in the current study.

Our results show that the spatial and temporal variability of surface meltwater reaching the ice-sheet bed provides a fundamental control on subglacial drainage system development. In the current study, this process was investigated by varying the areal density of moulins, which was controlled by a simple ice-fracture mechanism affecting the location and timing of lake drainage events.

The different moulin densities cause the subglacial drainage system to evolve in contrasting ways, creating different patterns of water pressure, which might be expected to generate different ice dynamic responses. For a high moulin density, the change from a predominantly distributed to channelized system occurs earlier in the melt season and over a larger area of the bed, than for the low moulin density scenario. This leads to a more rapid and widespread reduction in water pressure from earlier in the melt season, which might be expected to cause a decrease in early-season basal sliding and thus the total annual displacement of ice. The corollary of this, however, is that larger areas of the bed experience high diurnal water-pressure variations for longer throughout the late season for the high moulin density scenario compared to the low moulin density scenario, which might be expected to cause short-term increases in basal sliding at this time. The implications of all this for the overall summer and annual velocity regimes, both now and into the future, require further study.

In summary, our results suggest that although the intensity and areal extent of surface melt has a strong control on subglacial drainage development, water pressures and therefore ice velocities, moulin density is also of crucial importance as this controls where and when this meltwater can access the bed during the melt season.

Acknowledgments and Data

This work was funded through a UK Natural Environment Research Council Doctoral Training Grant (LCAG/133), a Bowring Junior Research Fellowship (St Catharine's College, Cambridge) and a Leverhulme/Newton Trust Early Career Fellowship, all awarded to A.F.B. I.J.H. was supported by a Marie Curie FP7 Career Integration Grant within the 7th European Union Framework Programme. We are very grateful to Dorthe Petersen for data from the Asiaq Greenland Survey, and to Konrad Steffen for GC-Net data. Requests to access the Asiaq Greenland Survey coastal precipitation and temperature data should be directed to Dorthe Petersen; see <http://www.asiaq.gl/en-us/knowledgeanddata/databaseandarchive.aspx>. The GC-Net climate data are available on request from <http://cires.colorado.edu/science/groups/steffen/gcnet/>. Finally, we thank the Editor, Bryn Hubbard, and three anonymous reviewers for their valuable contributions towards improving our

785 initial manuscript.

786 **References**

787 Andrews, L. C., Catania, G. A. Hoffmann, M. J. Gulley, J. D, Luthi, M. P. Ryser, C, Hawley, R. L,
788 and Neumann, T. A. (2014), Direct observations of evolving subglacial drainage beneath the
789 Greenland Ice Sheet, *Nature*, 514, 80–83, doi:10.1038/nature13796.

790 Arnold, N. S., Banwell, A. F., and Willis, I. C. (2014), High-resolution modelling of the seasonal
791 evolution of surface water storage on the Greenland Ice Sheet, *Cryosphere*, 8, 1149–1160,
792 doi:10.5194/tc-8-1149-2014.

793 Arnold, N. S. (2010), A new approach for dealing with depressions in digital elevation models when
794 calculating flow accumulation values, *Prog. Phys. Geogr.*, 34(6), 781–809,
795 doi:10.1177/0309133310384542.

796 Arnold, N., Richards, K., Willis, I. and Sharp, M (1998), Initial results from a distributed, physically
797 based model of glacier hydrology, *Hydrol. Processes*, 12, 191–219, doi:10.1002/(SICI)1099-
798 1085(199802)12:2<191:: AID-HYP571>3.0.CO;2-C.

799 Banwell, A. F., I. C. Willis, N. S. Arnold, A. Messerli, C. J. Rye and A. P. Ahlstrøm (2012a),
800 Calibration and validation of a high resolution surface mass balance model for Paakitsoq, west
801 Greenland, *J. Glaciol.*, 58(212), 1047–1062, doi:10.3189/2012JoG12J034.

802 Banwell, A. F., N. S. Arnold, I. C. Willis, M. Tedesco, and A. P Ahlstrom (2012b), Modelling
803 supraglacial water routing and lake filling on the Greenland Ice Sheet. 117 *J. Geophys. Res.*,
804 doi:10.1029/2012JF002393.

805 Banwell, A. F., I. Willis, and N. Arnold (2013), Modeling subglacial water routing at Paakitsoq, W
806 Greenland, *J. Geophys. Res. Earth Surf.*, 118, 1282–1295, doi:10.1002/jgrf.20093.

807 Banwell, A.F., Caballero, M., Arnold, N.S., Glasser, N.F., Cathles, L.M. and MacAyeal, D.R.
808 (2014). Supraglacial lakes on the Larsen B ice shelf, Antarctica, and at Paakitsoq, West Greenland:
809 A comparative study. *Annals of Glaciology*, 55, 1-8. doi:10.3189/2014AoG66A049.

810 Bartholomew, I., Nienow, P., Mair, D., Hubbard, A., King, M. A., and Sole, A. (2010), Seasonal
811 evolution of subglacial drainage and acceleration in a Greenland outlet glacier, *Nat. Geosci.*, 3, 408–
812 411.

813 Bartholomew, I., Nienow, P., Sole, A., Mair, D., Cowton, T., and King, M. (2012) Short-term
814 variability in Greenland Ice Sheet motion forced by time-varying meltwater drainage: Implications

815 for the relationship between subglacial drainage system behavior and ice velocity, *J. Geophys. Res.*
816 *Earth Surf.*, 117, F03002, doi:10.1029/2011JF002220.

817 Bartholomaeus, T. C., R. S. Anderson, and S. P. Anderson (2011), Growth and collapse of the
818 distributed subglacial hydrologic system of Kennicott Glacier, Alaska, USA, and its effects on basal
819 motion, *J. Glaciol.*, 57(206), 985–1002, doi:10.3189/002214311798843269.

820 Bougamont, M., Christoffersen, P., Hubbard, A.L., Fitzpatrick, A.A., Doyle, S.H. and Carter, S. P.,
821 (2014). Sensitive response of the Greenland Ice Sheet to surface melt drainage over a soft bed. *Nat*
822 *Commun*, v. 5, p.5052-5052. doi:10.1038/ncomms6052.

823 Catania, G. A., and Neumann, T. A. (2010), Persistent englacial drainage features in the Greenland
824 ice sheet, *Geophys. Res. Lett.*, 37, L02501, doi:10.1029/2009GL041108.

825 Catania, G. A., Neumann, T. A. and Price, S. F., (2008), Characterizing englacial drainage in the
826 ablation zone of the Greenland ice sheet, *J. Glaciol.*, 54(187), 567–578,
827 doi:10.3189/002214308786570854.

828 Clason, C., Mair, D. W. F., Burgess, D. O., and Nienow, P. W. (2012) Modelling the delivery of
829 supraglacial meltwater to the ice/bed inter- face: Application to southwest Devon Ice Cap, Nunavut,
830 Canada, *J. Glaciol.*, 58, 361–374, doi:10.3189/2012JoG11J129.

831 Chandler, D. M., et al. (2013), Evolution of the subglacial drainage system beneath the Greenland ice
832 sheet revealed by tracers, *Nat. Geosci.*, 6(3), 195–198.

833 Chu, W., T. T. Creyts, and R. E. Bell (2016), Rerouting of Subglacial Water Flow between
834 Neighboring Glaciers in West Greenland. *J. Geophys. Res. Earth Surf.*, 120, doi:
835 10.1002/2015JF003705.

836 Church, J. A., *et al.* (2013), Sea level change, in *Climate Change 2013: The Physical Science Basis.*
837 Contribution of Working Group I to the Fifth Assessment Report of the Intergovernmental Panel on
838 Climate Change, edited by T. F. Stocker et al., Cambridge Univ. Press, Cambridge, U. K., and New
839 York.

840 Colgan, W., and Steffen. K. (2009), Modeling the spatial distribution of moulins near Jakobshavn,
841 Greenland, IOP Conf. Ser.: *Earth Environ. Sci.*, 6, 012022, doi:10.1088/1755-1307/6/1/012022.

842 Colgan, W., H. Rajaram, R. Anderson, K. Steffen, T. Phillips, I. Joughin, H. J. Zwally, and W.
843 Abdalati (2011), The annual glaciohydrology cycle in the ablation zone of the Greenland ice sheet:
844 Part 1. Hydrology model, *J. Glaciol.*, 57(204), 697–709, doi:10.3189/002214311797409668.

845 Colgan, W., H. Rajaram, R. S. Anderson, K. Steffen, H. J. Zwally, T. Phillips, and W. Abdalati
846 (2012), The annual glaciohydrology cycle in the ablation zone of the Greenland ice sheet: Part 2.
847 Observed and modeled ice flow, *J. Glaciol.*, 58(207), 51–64, doi:10.3189/2012JoG11J081.

848 Cowton, T., P. Nienow, A. Sole, J. Wadham, G. Lis, I. Bartholomew, D. Mair, and D. Chandler
849 (2013), Evolution of drainage system morphology at a land-terminating Greenlandic outlet glacier, *J.*
850 *Geophys. Res. Earth Surf.*, 118(1), 29–41, doi:10.1029/2012JF002540.

851 Das, S. B., I. Joughin, M. D. Behn, I. M. Howat, M. A. King, and D. Lizarralde (2008), Fracture
852 propagation to the base of the Greenland ice sheet during supraglacial lake drainage, *Science*, 320,
853 778–781, doi:10.1126/science.1153360.

854 de Fleurian, B., O. Gagliardini, T. Zwinger, G. Durand, E. Le Meur, D. Mair, and P. Råback (2014),
855 A double continuum hydrological model for glacier applications, *The Cryosphere*, 8(1), 137–153,
856 doi:10.5194/tc-8-137-2014.

857 Doyle, S. H., Hubbard, A. L., Dow, C. F., Jones, G. A., Fitzpatrick, A., Gusmeroli, A., Kulessa, B.,
858 Lindback, K., Pettersson, R., and Box, J. E. (2013), Ice tectonic deformation during the rapid in situ
859 drainage of a supraglacial lake on the Greenland Ice Sheet, *Cryosphere*, 7, 129–140, doi:10.5194/tc-
860 7-129-2013.

861 Doyle, S., Hubbard, A., van de Wal, R., Box, J., van As, D., Scharrer, K., Meierbachtol, T., Smeets,
862 P., Harper, J., Johansson, E., Mottram, R., Mikkelsen, A., Wilhelms, F., Patton, H., Christoffersen,
863 P., Hubbard, B. (2015), Amplified melt and flow of the Greenland ice sheet driven by late-summer
864 cyclonic rainfall. *Nature Geoscience* 10.1038/NGEO2482

865 Dow, C. F., Kulessa, B., Rutt, I. C., Doyle, S. H., and Hubbard, A. (2014), Upper bounds on
866 subglacial channel development for interior regions of the Greenland ice sheet, *J. Glaciol.*, 60(224),
867 1044–1052.

868 Dow, C. F. et al. (2015), Modeling of subglacial hydrological development following rapid
869 supraglacial lake drainage, *J. Geophys. Res. Earth Surf.*, 120(6), 2014JF003333,
870 doi:10.1002/2014JF003333.

871 Flowers, G.E., Clarke, G.K.C., (2002). A multicomponent coupled model of glacier hydrology 1.
872 Theory and synthetic examples. *J. Geophys. Res.* 107.

873 Graversen, R. G., S. Drijfhout, W. Hazeleger, R. van de Wal, R. Bintanja, and M. Hersen (2011),
874 Greenland's contribution to global sea-level rise by the end of the 21st century, *Clim. Dyn.*, 37(7–8),
875 1427–1442, doi:10.1007/s00382-010-0918-8.

876 Gulley, J.D., Walthard, P., Martin, J., Banwell, A.F., Benn, D.I. and Catania, G., 2012. Conduit
 877 roughness and dye-trace breakthrough curves: Why slow velocity and high dispersivity may not
 878 reflect flow in distributed systems. *Journal of Glaciology*, v. 58, p.915-925.
 879 [doi:10.3189/2012JoG11J115](https://doi.org/10.3189/2012JoG11J115).

880 Hanna, E., et al. (2013), Ice-sheet mass balance and climate change, *Nature*, 498(7452), 51–9,
 881 [doi:10.1038/nature12238](https://doi.org/10.1038/nature12238).

882 Hewitt, I. J. (2013), Seasonal changes in ice sheet motion due to melt water lubrication, *Earth*
 883 *Planet. Sci. Lett.*, 371–372, 16–25, [doi:10.1016/j.epsl.2013.04.022](https://doi.org/10.1016/j.epsl.2013.04.022).

884 Hoffman, M. J., G. A. Catania, T. A. Neumann, L. C. Andrews, and J. A. Rumrill (2011), Links
 885 between acceleration, melting, and supraglacial lake drainage of the western Greenland Ice Sheet, *J.*
 886 *Geophys. Res.: Earth Surf.* 116, F04035, [doi:10.1029/2010JF001934](https://doi.org/10.1029/2010JF001934).

887 Hoffman, M., and S. Price (2014), Feedbacks between coupled subglacial hydrology and glacier
 888 dynamics, *J. Geophys. Res. Earth Surf.*, 119(3), 414–436, [doi:10.1002/2013JF002943](https://doi.org/10.1002/2013JF002943).

889 Hubbard, B. P., M. J. Sharp, I. C. Willis, M. K. Nielsen, and C. C. Smart (1995), Borehole water-
 890 level variation and the structure of the subglacial hydrological system of Haut Glacier d'Arolla,
 891 Valais, Switzerland, *J. Glaciol.*, 41(139), 572–583.

892 Krawczynski, M. J., M. D. Behn, S. B. Das, and I. Joughin (2009), Constraints on lake volume
 893 required for hydro-fracture through ice sheets, *Geophys. Res. Lett.*, 36, L10501,
 894 [doi:10.1029/2008GL036765](https://doi.org/10.1029/2008GL036765).

895 Leeson, A. A., A. Shepherd, K. Briggs, I. Howat, X. Fettweis, M. Morlighem, and E. Rignot (2014),
 896 Supraglacial lakes on the Greenland ice sheet advance inland under warming climate, *Nat. Clim.*
 897 *Change*, 5(1), 51–55, [doi:10.1038/nclimate2463](https://doi.org/10.1038/nclimate2463).

898 Lindbäck, K., R. Pettersson, A. L. Hubbard, S. H. Doyle, D. van As, A. B. Mikkelsen, and A. A.
 899 Fitzpatrick (2015), Subglacial water drainage, storage, and piracy beneath the Greenland ice sheet,
 900 *Geophys. Res. Lett.*, 2015GL065393, [doi:10.1002/2015GL065393](https://doi.org/10.1002/2015GL065393).

901 Lüthi, M. P., M. Funk, A. Iken, S. Gogineni, and M. Truffer (2002), Mechanisms of fast flow in
 902 Jakobshavns Isbrae, Greenland; Part III: Measurements of ice deformation, temperature and cross-
 903 borehole conductivity in boreholes to the bedrock, *J. Glaciol.*, 48(162), 369–385,
 904 [doi:10.3189/172756502781831322](https://doi.org/10.3189/172756502781831322).

905 Mayaud, J. R., A. F. Banwell, N. S. Arnold, and I. C. Willis (2014), Modeling the response of
 906 subglacial drainage at Paakitsoq, west Greenland, to 21st century climate change, *J. Geophys. Res.*
 907 *Earth Surf.*, 119, doi:10.1002/ 2014JF003271.

908 Meierbachtol, T., J. Harper, and N. Humphrey (2013), Basal Drainage System Response to
 909 Increasing Surface Melt on the Greenland Ice Sheet, *Science*, 341(6147), 777–779,
 910 doi:10.1126/science.1235905.

911 McMillan, M., P. Nienow, A. Shepherd, T. Benham, and A. Sole (2007), Seasonal evolution of
 912 supra-glacial on the Greenland Ice Sheet, *Earth Planet. Sci. Lett.*, 262, 484–492,
 913 doi:10.1016/j.epsl.2007.08.002.

914 Nienow, P., M. Sharp, and I. Willis (1998), Seasonal changes in the morphol- ogy of the subglacial
 915 drainage system, Haut Glacier d'Arolla, Switzerland, *Earth Surf. Processes Landforms*, 23, 825–843,
 916 doi:10.1002/(SICI)1096- 9837(199809)23:9<825::AID-ESP893>3.0.CO;2-2.

917 Palmer, S. J., A. Shepherd, P. Nienow, and I. Joughin (2011), Seasonal speedup closely correlated
 918 with surface hydrology at the western margin of the Greenland Ice Sheet, *Earth Planet. Sci. Lett.*,
 919 302(3–4), 423–428, doi:10.1016/j.epsl.2010.12.037.

920 Pimentel, S., and G. Flowers (2010), A numerical study of hydrologically driven glacier dynamics
 921 and subglacial flooding, *Proc. R. Soc. A*, 467(2126), 37–558, doi:10.1098/rspa.2010.0211.

922 Plummer, J., S. Gogineni, C. van der Veen, C. Leuschen, and J. Li (2008), Ice thickness and bed map
 923 for Jakobshavn Isbræ, *Center for Remote Sensing of Ice Sheets Technical Report*.

924 Poinar, K., I. Joughin, S. B. Das, M. D. Behn, J. T. M. Lenaerts, and M. R. van den Broeke (2015),
 925 Limits to future expansion of surface-melt-enhanced ice flow into the interior of western Greenland,
 926 *Geophys. Res. Lett.*, 42(6), 2015GL063192, doi:10.1002/2015GL063192.

927 Röthlisberger, H. and Iken, A. (1981), Plucking as an effect of water pressure variations at the
 928 glacier bed. *Ann. Glaciol.* 2, 57-62.

929 Ryser, C., Lüthi, M. P., Andrews, L. C., Hoffman, M. J., Catania, G. A., Hawley, R. L., Neumann, T.
 930 A., Kristensen, S. S., (2014), Sustained high basal motion of the Greenland Ice Sheet revealed by
 931 borehole deformation. *J. Glaciol.* 60, 647–660

932 Schoof, C. (2010), Ice-sheet acceleration driven by melt supply variability, *Nature*, 468, 803–806,
 933 doi:10.1038/nature09618.

934 Selmes, N., T. Murray, T. D. and James, (2013), Characterizing supraglacial lake drainage on the
 935 Greenland ice sheet. *The Cryosphere Discuss*, 7, 475–505. doi:10.5194/tcd-7-475-2013.

936 Sharp, M., K. Richards, I. Willis, N. Arnold, P. Nienow, W. Lawson, and J.-L. Tison (1993),
 937 Geometry, bed topography and drainage system structure of the haut glacier d'Arolla, Switzerland,
 938 *Earth Surf. Processes Landforms*, 18, 557–571, doi:10.1002/esp.3290180608.

939 Shepherd, A., Hubbard, A., Nienow, P., King, M., McMillan, M., and Joughin, I. (2009) Greenland
 940 ice sheet motion coupled with daily melting in late summer, *Geophys. Res. Lett.*, 36, L01501,
 941 doi:10.1029/2008GL035758.

942 Shreve, R. (1972), Movement of water in glaciers, *J. Glaciol.*, 11(62), 205–214.

943 Smith, L. C. et al. (2015), Efficient meltwater drainage through supraglacial streams and rivers on
 944 the southwest Greenland ice sheet, *Proc. Natl. Acad. Sci.*, 112(4), 1001– 1006,
 945 doi:10.1073/pnas.1413024112.

946 Spring, U., and K. Hutter (1981), Numerical studies of Jokulhlaups, *Cold Reg. Sci. Technol.*, 4, 227–
 947 244, doi:10.1016/0165-232X(81)90006-9.

948 Steffen, K., and J. Box (2001), Surface climatology of the Greenland ice sheet: Greenland Climate
 949 Network 1995–1999, *J. Geophys. Res. Atmos.*, 106(D24), 33951–33964.

950 Stevens, L. A., Behn, M.D., McGuire, J.J., Das, S.B., Joughin, I., Herring, T., Shean, D.E. and King,
 951 M.A. (2015), Greenland supraglacial lake drainages triggered by hydrologically induced basal slip.
 952 *Nature* 522, 73-76; doi: 10.1038/nature14480

953 Sundal, A. V., A. Shepherd, P. Nienow, E. Hanna, S. Palmer, and P. Huybrechts (2011), Melt-
 954 induced speed-up of Greenland Ice Sheet offset by efficient subglacial drainage, *Nature*, 469, 522–
 955 U83, doi:10.1038/ nature09740.

956 Tedesco, M., I. C. Willis, M. J. Hoffman, A. F. Banwell, P. Alexander, and N. S. Arnold (2013), Ice
 957 dynamic response to two modes of surface lake drainage on the Greenland ice sheet, *Environ. Res.*
 958 *Lett.*, 8(3), 34,007, doi:10.1088/1748-9326/8/3/034007.

959 Tedstone, A. J. et al. (2013), Greenland ice sheet motion insensitive to exceptional meltwater
 960 forcing. *Proc. Natl Acad. Sci. USA* 110, 19719–19724.

961 Tedstone, A J, Nienow, P W, Gourmelen, N, Dehecq, A, Goldberg, D and Hanna, E (2015), Decadal
 962 slowdown of a land-terminating sector of the Greenland Ice Sheet despite warming. *Nature Reviews.*
 963 526., 692-695 doi:10.1038/nature15722

964 Thomsen, H. H., and O. B. Olesen (1989), Applied glacier research for planning hydro-electric
 965 power, Ilulissat/Jakobshavn, West Greenland, *Ann. Glaciol.*, 13, 257–261.

966 Thomsen, H., O. Olesen, R. J. Braithwaite, and C. Boggild (1991), Ice drilling and mass balance at
 967 Pakitsoq, Jakobshavn, central West Greenland, *Groenl. Geol. Unders.*, Copenhagen, 152.

968 van As, D., A. L. Hubbard, B. Hasholt, A. B. Mikkelsen, M. R. van den Broeke, and R. S. Fausto
 969 (2012), Large surface meltwater discharge from the Kangerlussuaq sector of the Greenland Ice Sheet
 970 during the record-warm year 2010 explained by detailed energy balance observations, *Cryosphere*,
 971 6(1), 199–209, doi:10.5194/tc-6-199-2012.

972 van der Veen, C. J. (2007), Fracture propagation as means of rapidly transferring surface meltwater
 973 to the base of glaciers, *Geophys. Res. Lett.*, 34, L01501, doi:10.1029/2006GL028385.

974 van de Wal, R. S. W., W. Boot, M. R. van den Broeke, C. J. P. P. Smeets, C. H. Reijmer, J. J. A.
 975 Donker, and J. Oerlemans (2008), Large and rapid melt-induced velocity changes in the ablation
 976 zone of the Greenland Ice Sheet, *Science*, 321, 111–113, doi:10.1126/science.1158540.

977 van de Wal, R. S. W., Smeets, C. J. P. P., Boot, W., Stoffelen, M., van Kampen, R., Doyle, S. H.,
 978 Wilhelms, F., van den Broeke, M. R., Reijmer, C. H., Oerlemans, J., and Hubbard, A (2015) Self-
 979 regulation of ice flow varies across the ablation area in south-west Greenland, *Cryosphere*, 9, 603-
 980 611, doi:10.5194/tc-9-603-2015.

981 Vaughan, D. G., et al. (2013), Observations: Cryosphere, in Climate Change 2013: The Physical
 982 Science Basis. Contribution of Working Group I to the Fifth Assessment Report of the
 983 Intergovernmental Panel on Climate Change, edited by T. F. Stocker et al., Cambridge Univ. Press,
 984 Cambridge, U. K., and New York.

985 Werder, M. A., Hewitt, I. J., Schoof, C. J. and Flowers, G. E. (2013), Modeling channelized and
 986 distributed subglacial drainage in two dimensions, *J. Geophys. Res. Earth Surf.*, 118, 2140–2158,
 987 doi:10.1002/jgrf.20146.

988 Willis, I. C., Arnold, N. S. and Brock, B. W. (2002), Effect of snowpack removal on energy balance,
 989 melt and runoff in a small supraglacial catchment. *Hydrol. Proc.*, 16, 2721-2749,
 990 doi:10.1002/hyp.1067

991 Wright, P. J., J. T. Harper, N. F. Humphrey, and T. W. Meierbachtol (2016), Measured basal water
 992 pressure variability of the western Greenland Ice Sheet: Implications for hydraulic potential, *J.*
 993 *Geophys. Res. Earth Surf.*, 121, doi:10.1002/ 2016JF003819.

994 Yang, K., L. C. Smith, V. W. Chu, C. J. Gleason, and M. Li (2015), A Caution on the Use of Surface
995 Digital Elevation Models to Simulate Supraglacial Hydrology of the Greenland Ice Sheet, *IEEE J.*
996 *Sel. Top. Appl. Earth Obs. Remote Sens.*, 1–13, doi:10.1109/JSTARS.2015.2483483.

997 Zwally, H.J., Abdalati, W., Herring, T., Larson, K., Saba, J., and Steffen, K. (2002), Surface melt-
998 induced acceleration of Greenland ice-sheet flow, *Science*, 297, 218–222.

999 **Tables**

σ	K_s (Pa ⁻¹ s ⁻¹)	$\Sigma Mo - \Sigma Me$ as % of ΣMe discharge	RMSE (m ³ s ⁻¹)	Nash Sutcliffe coef.
1 x 10 ⁻⁴	1 x 10 ⁻⁶	-9.7	20.5	0.66
1 x 10⁻⁴	1 x 10⁻⁵	-0.5	19.7	0.68
1 x 10 ⁻⁴	1 x 10 ⁻⁴	-1.8	18.4	0.72
1 x 10 ⁻³	1 x 10 ⁻⁶	-2.1	25.1	0.49
1 x 10 ⁻³	1 x 10 ⁻⁵	-0.8	18.4	0.72
1 x 10 ⁻³	1 x 10 ⁻⁴	-2.7	18.3	0.72
1 x 10 ⁻²	1 x 10 ⁻⁶	4.5	29.7	0.28
1 x 10 ⁻²	1 x 10 ⁻⁵	-14	23.8	0.54
1 x 10 ⁻²	1 x 10 ⁻⁴	-15	21.3	0.63

1000

1001 Table 1. Differences between the total modeled (ΣMo) and measured (ΣMe ; $4.45 \times 10^8 \text{ m}^3$)
1002 proglacial discharges as a percentage of ΣMe for various combinations of parameter values for σ and
1003 K_s for the ‘optimum’ moulin density scenario ($F_a = 1000 \text{ m}^2$ from *Banwell et al.* [2013]). Root Mean
1004 Square Errors (RMSEs) and Nash–Sutcliffe model efficiency coefficients between the modeled and
1005 measured daily mean proglacial discharge time series are also given (NB. mean seasonal measured
1006 proglacial daily discharge = $44.0 \text{ m}^3 \text{ s}^{-1}$). The row in bold indicates the chosen parameter
1007 combination.

Lake number	Drainage date		
	LOW moulin density	‘Optimum’ moulin density	HIGH moulin density
646	17 May	-	-
624	17 May	18 May	-
619	17 May	-	-
602	16 May	16 May	17 May
600	18 May	-	-
582	19 May	21 May	-
581	18 May	-	-
578	31 May	-	-
572	21 May	10 June	-

564	19 May	-	-
559	18 May	-	-
551	19 May	1 June	10 June
532	21 May	7 June	12 June
528	20 May	-	-
494	3 June	-	-
468	11 June	17 June	4 July
446	15 June	18 June	-
444	9 June	12 June	18 June

1008

1009 Table 2. Drainage dates of lakes for each of the three moulin density scenarios: i) low ($F_a = 2500$
1010 m^2); ii) optimum ($F_a = 1000 \text{ m}^2$ from *Banwell et al.* [2013]); and iii) high ($F_a = 250 \text{ m}^2$). Lake
1011 locations are shown in Figure 2

1012 Figure Captions

1013 Figure 1. The model domain, which is identical to the subglacial catchment defined by *Banwell et al.*
1014 [2013]. The shading represents ice thickness, and the black contour lines depict the surface ice
1015 elevation. The inset shows the location of Paakitsoq in West Greenland (red box); $\sim 30 \text{ km}$ north of
1016 Jakobshavn Isbræ. The triangle marks the Asiaq proglacial gauging station and the stars show two of
1017 the GC-Net weather stations. (See *Banwell et al.*, 2013, their Figure 1, for the precise catchment
1018 location).

1019 Figure 2. The subglacial flow accumulation map for the model domain (as defined by *Banwell et al.*
1020 [2013]). Moulin locations for the *maximum* ($F_a = 0 \text{ m}^2$), *high* ($F_a = 250 \text{ m}^2$), ‘*optimum*’ ($F_a = 1000$
1021 m^2 , from *Banwell et al.* [2013]) and *low* ($F_a = 2500 \text{ m}^2$) moulin density scenarios are indicated by: i)
1022 black dots; ii) white circles; iii) white stars; and iv) red stars, respectively. Lake/moulin numbers
1023 (which are equivalent) are indicated in white text. The triangle marks the Asiaq gauging station.
1024 (Figure adapted from *Banwell et al.* [2013].) Dates of lake drainage events for the various scenarios
1025 are given in Table 2.

1026 Figure 3. Time series of P_w/P_i for 8 moulins showing results of both the current study and that of
1027 *Banwell et al.* [2013] for the ‘optimum’ moulin density scenario ($F_a = 1000 \text{ m}^2$). (a) Highlights four
1028 moulins that experience short-term ($< 24 \text{ h}$) spikes in water pressure; while (b) highlights four
1029 moulins that experience periods of sustained high water pressure (see Figure 2 for lake/moulin
1030 locations). The timings of lake drainage events are shown along the x-axes of each plot. The black
1031 horizontal dashed lines show where $P_w/P_i = 1$.

1032 Figure 4. Daily mean width-integrated subglacial water discharge ($\text{m}^2 \text{ s}^{-1}$) (left column) and daily
1033 mean P_w/P_i (right column) on a sequence of days through the 2005 melt season across the subglacial
1034 domain for the (a) low; and (b) high moulin density scenarios. The solid black dots indicate moulins
1035 that are closed (i.e. ‘potential moulins’), and the open black circles indicate moulins that are open
1036 (i.e. those that are receiving water), with their size proportional to the surface water discharge
1037 entering the moulin. In the left column, the intensity of blue shading represents the subglacial
1038 discharge, and the red contour lines indicate hydraulic equipotential. In the right column, the
1039 intensity of red shows P_w/P_i , with $P_w/P_i = 0$ indicative of water at atmospheric pressure, and $P_w/P_i =$
1040 1 indicative of water at ice overburden pressure.

1041 Figure 5: Mean P_w/P_i over the melt season for the (a) low; and (b) high moulin density scenarios, and
1042 (c) the difference between the low and high moulin density scenarios (low *minus* high moulin
1043 density). Moulin locations are shown in Figure 2.

1044 Figure 6. The number of days out of the 113 day melt season where $P_w/P_i \geq 1$ for the (a) low; (c)
1045 high; and (e) maximum moulin density scenarios, and the number of days out of the 113 day melt
1046 season where the diurnal range in $P_w/P_i \geq 0.2$ for the (b) low; (d) high; and (f) maximum moulin
1047 density scenarios. Moulin locations are shown in Figure 2.

1048

Figure 1.

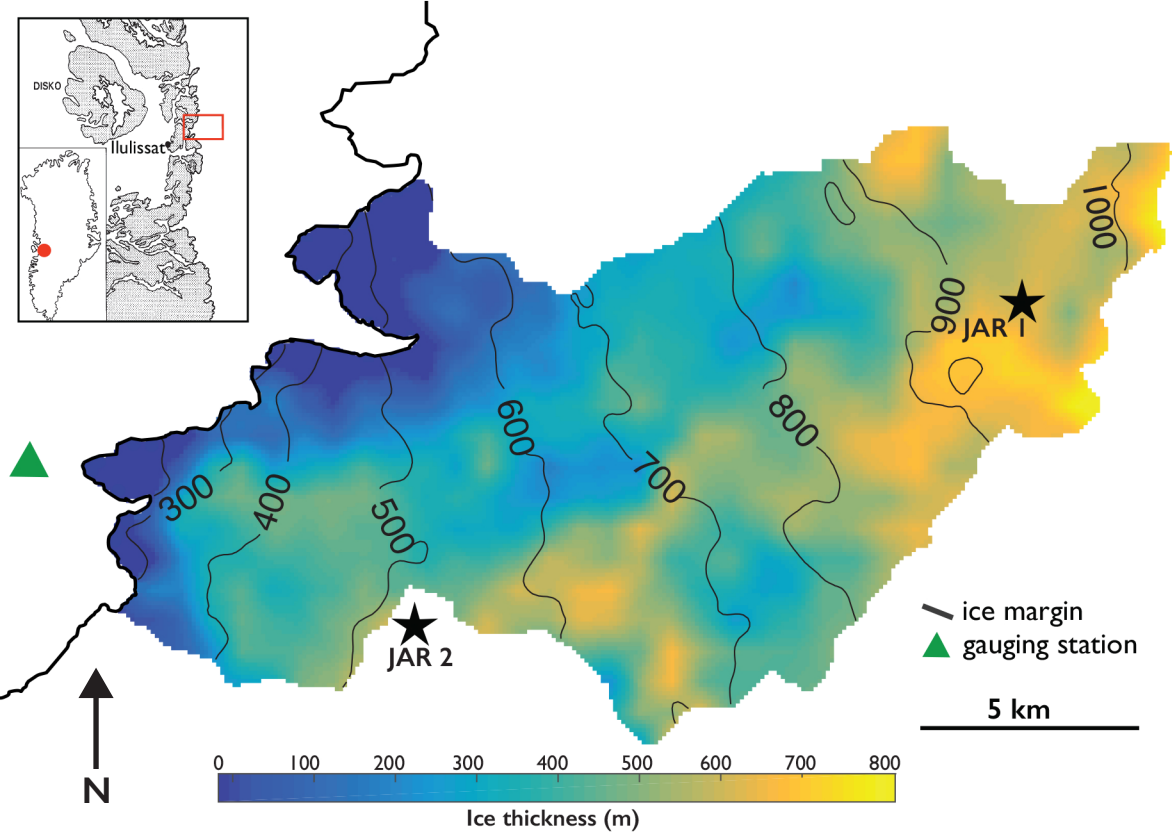


Figure 2.

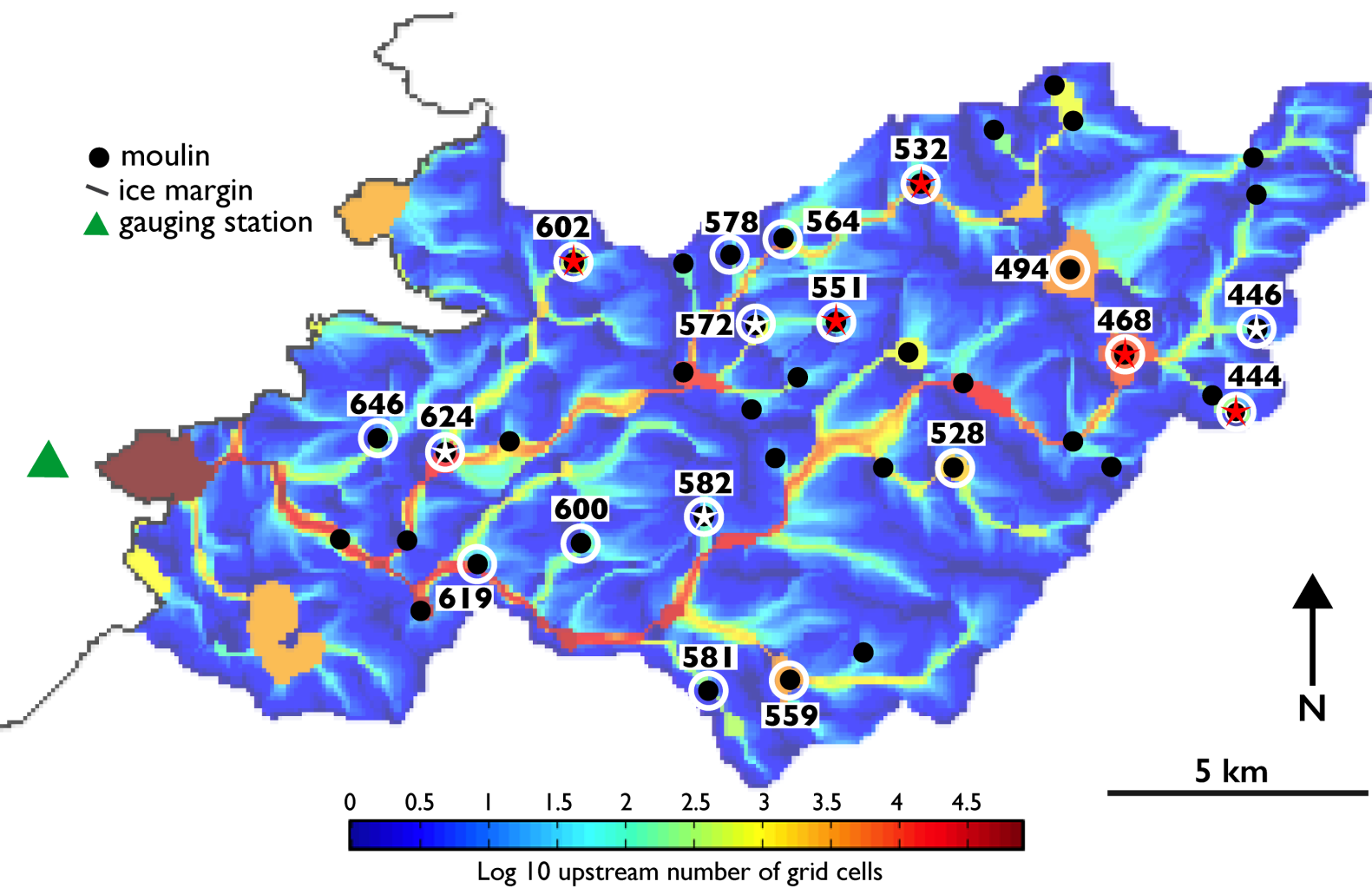


Figure 3.

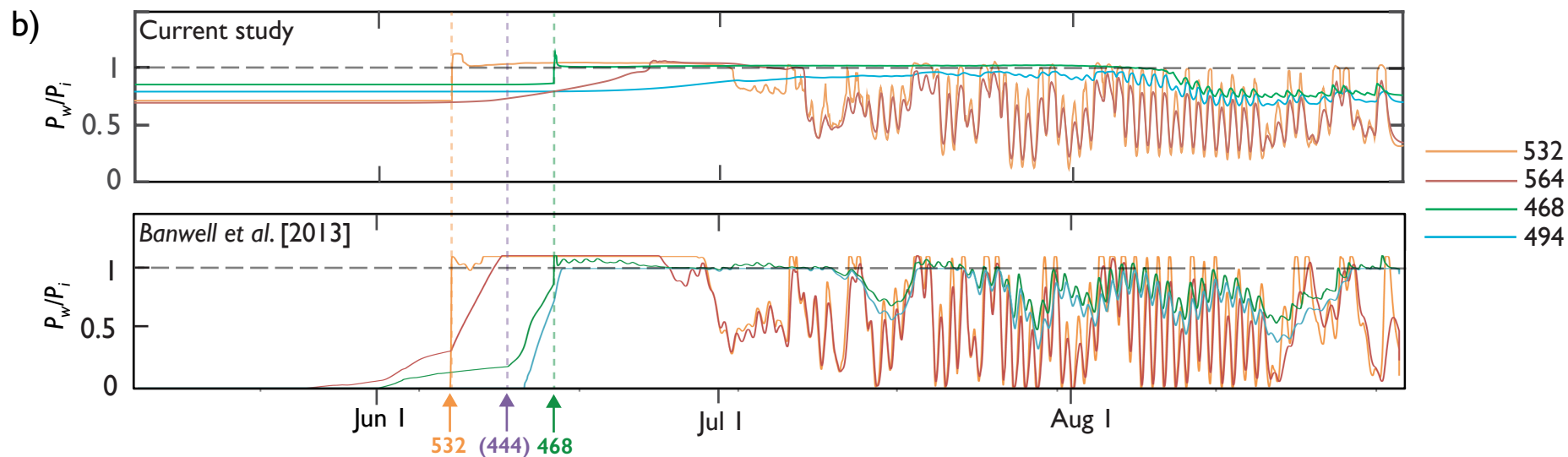
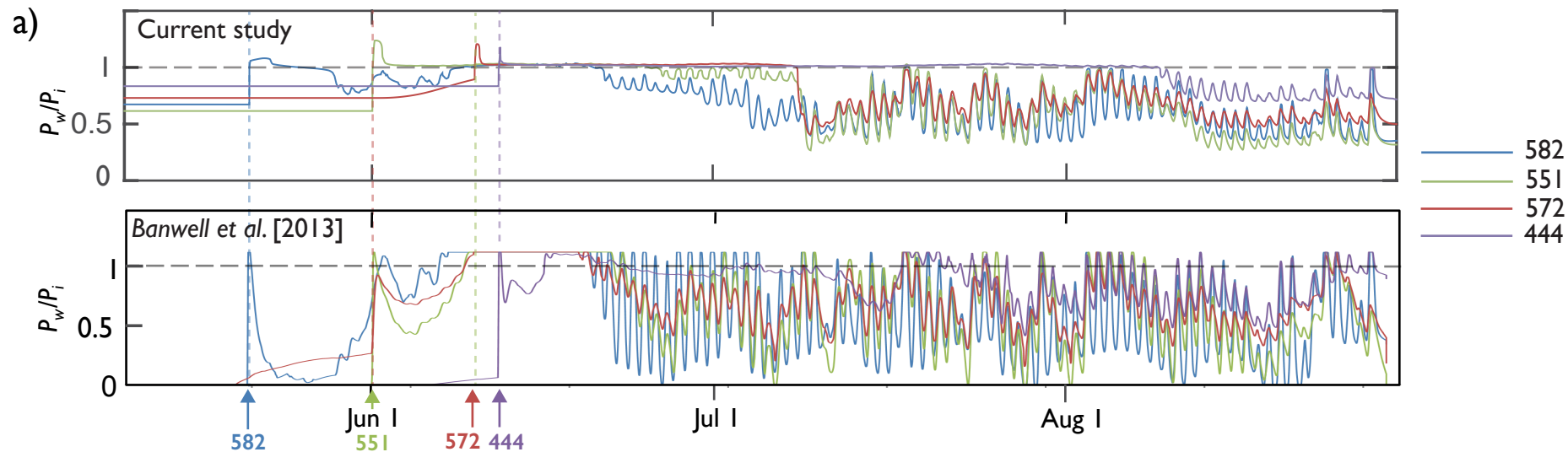


Figure 4a.

a)

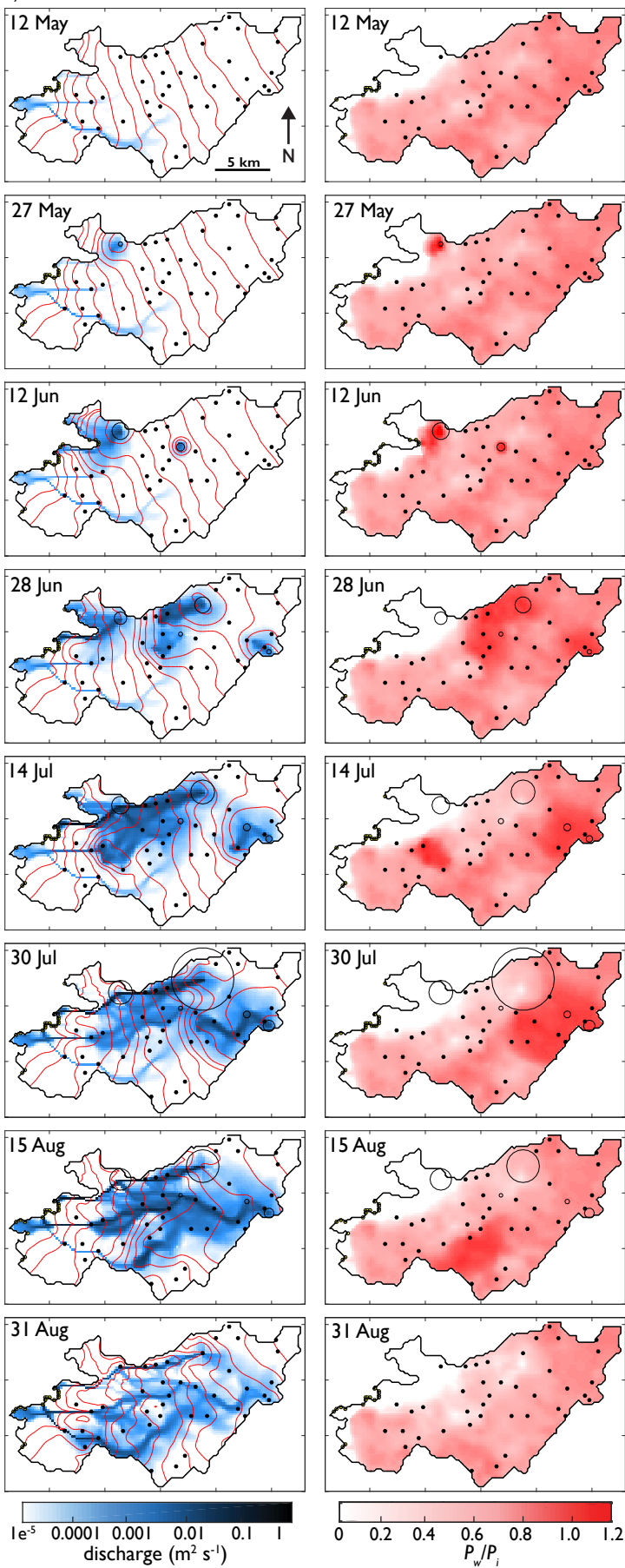


Figure 4b.

b)

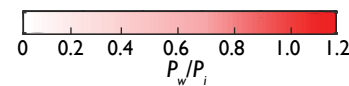
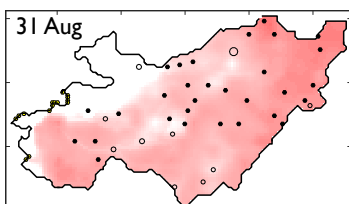
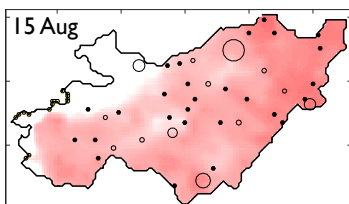
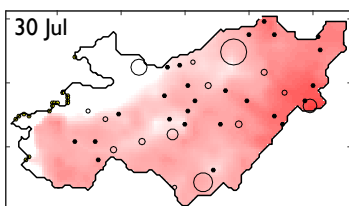
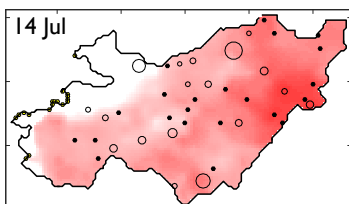
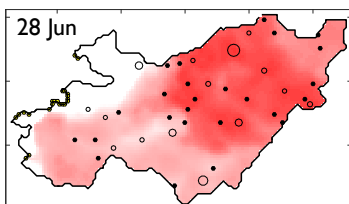
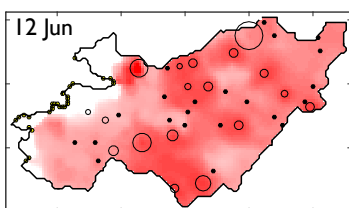
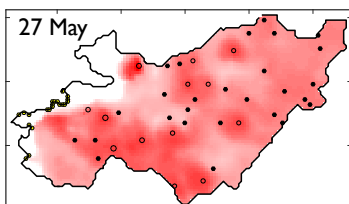
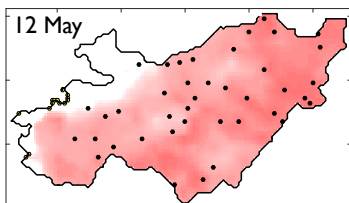
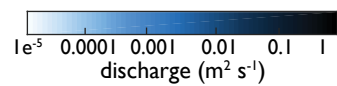
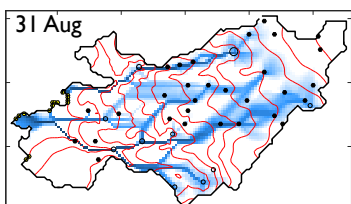
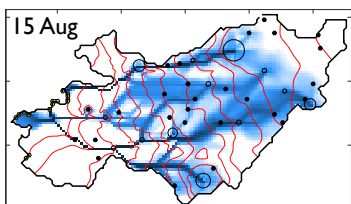
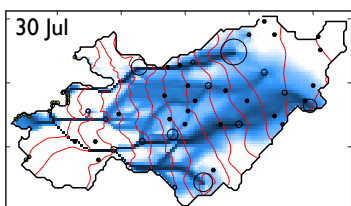
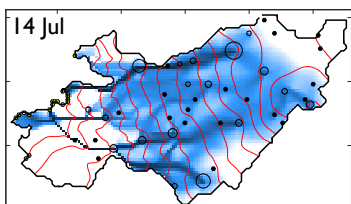
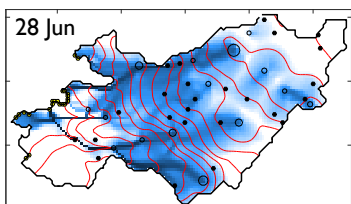
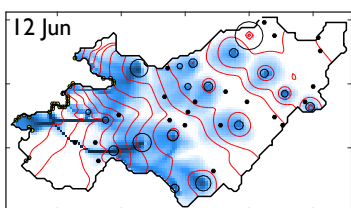
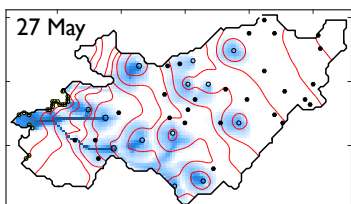
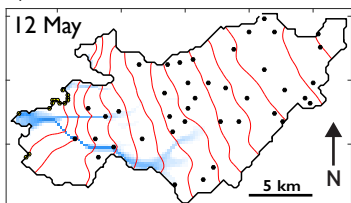


Figure 5.

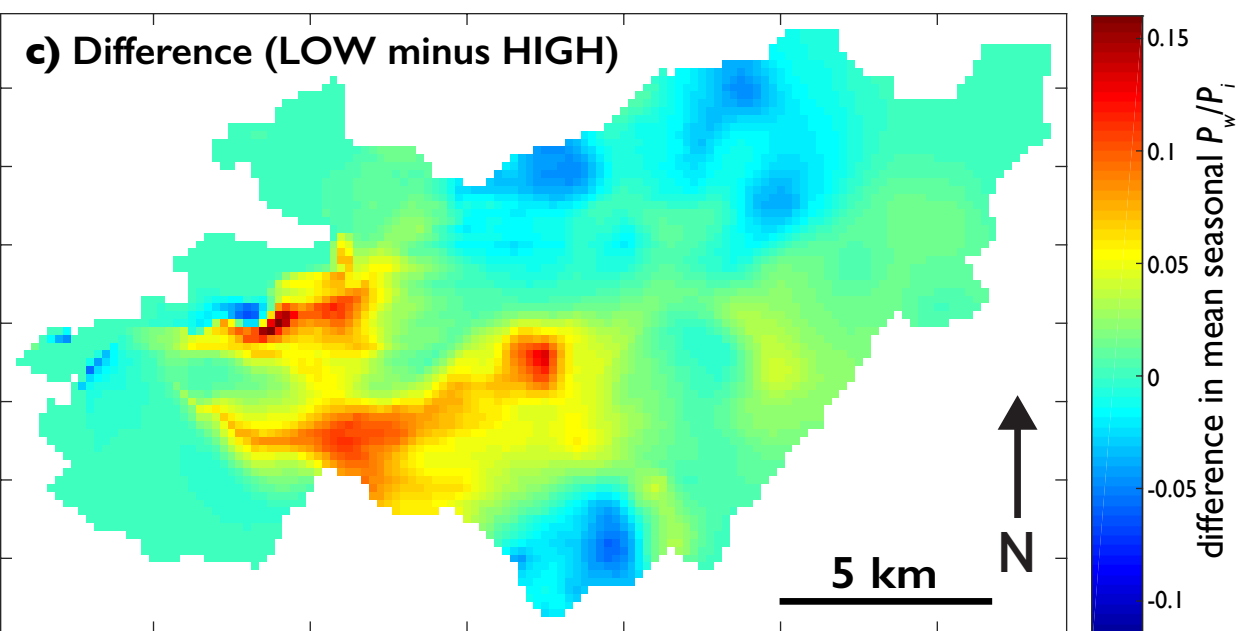
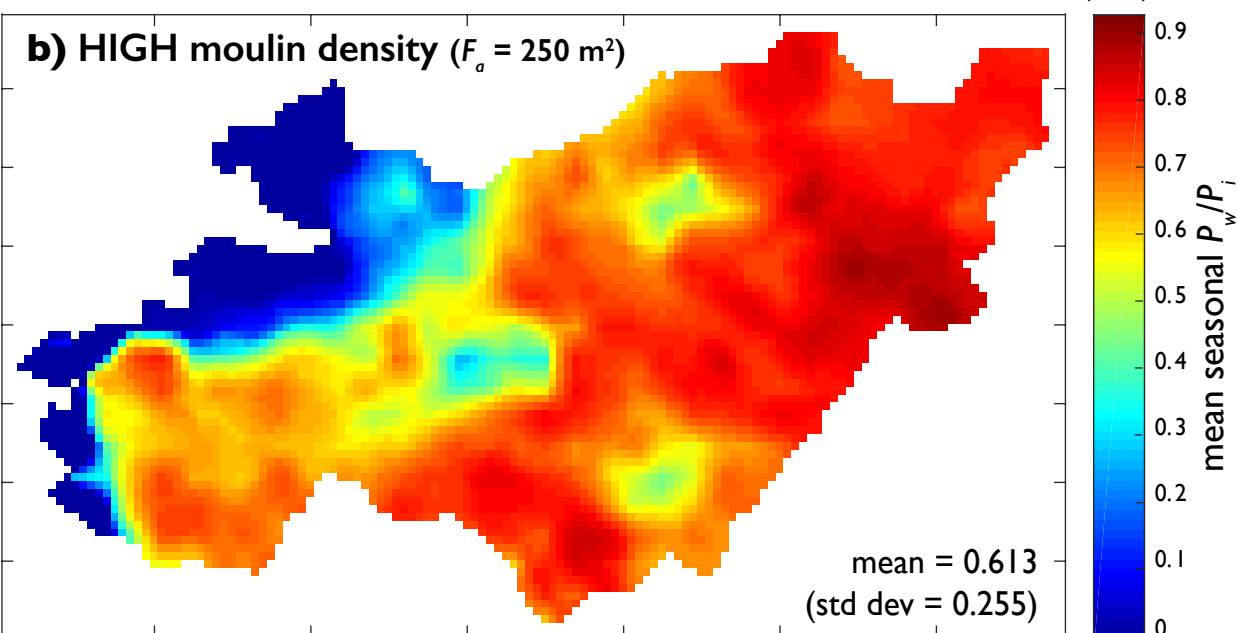
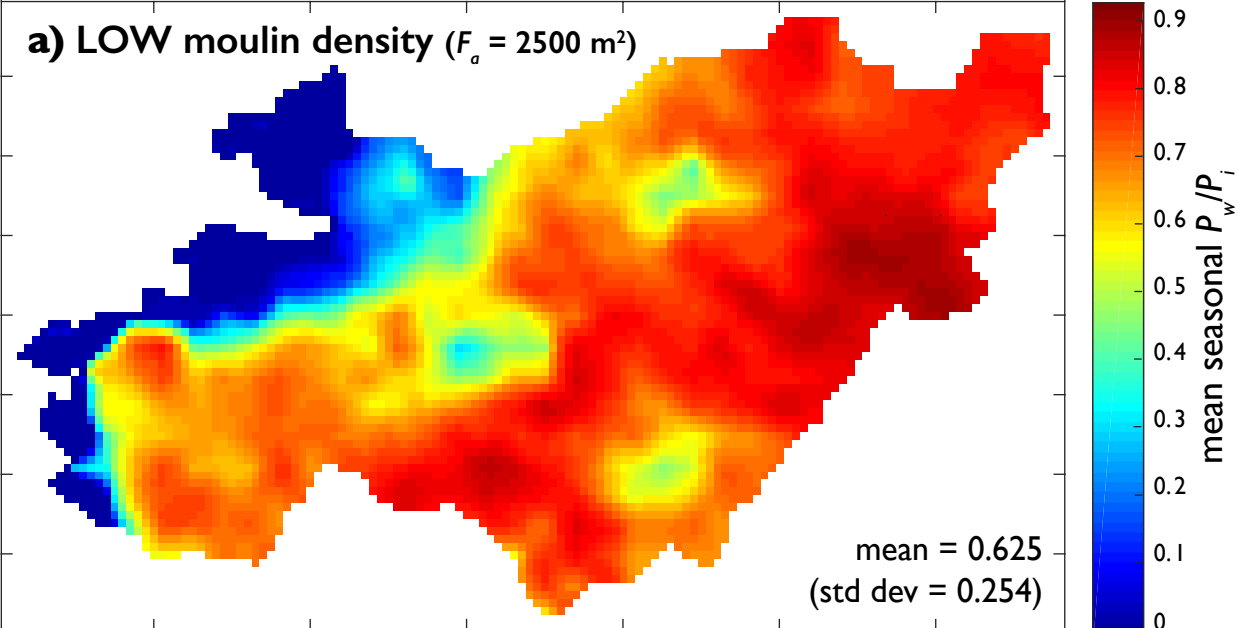


Figure 6.

